Neutron Irradiation Damage to the Metallic Components of UWCTR Magnet System

P. Sanger

February 1973

UWFDM-34

FUSION TECHNOLOGY INSTITUTE

UNIVERSITY OF WISCONSIN

MADISON WISCONSIN

Neutron Irradiation Damage to the Metallic Components of UWCTR Magnet System

P. Sanger

Fusion Technology Institute
University of Wisconsin
1500 Engineering Drive
Madison, WI 53706

http://fti.neep.wisc.edu

February 1973

UWFDM-34

Neutron Irradiation Damage to the Metallic Components of UWCTR Magnet System

by

Phillip A. Sanger

February 1973

FDM-34

I. INTRODUCTION

One of the prerequisites for the successful operation of a fusion reactor is a reliable operation of the superconducting magnet system. This reliability must be guaranteed even after many years of service in a particle radiation field. It is therefore, necessary to evaluate the radiation damage that can be expected during the lifetime of the reactor.

Any cryogenic superconducting magnet will in general make demands of both metallic and non-metallic materials. In the metallic category, materials for three different functions are needed: a) superconductor (NbTi or Nb_3Sn) b) stabilizer (Cu or Al) and c) structure (304 SS). In the UWCTR magnet, these components occupy respectively 1%, 32% and 67% by volume.[1,2] The non-metallic materials play structural, thermal, and electrical roles. A mineral-filled epoxy will be used to mechanically bond the copper to the steel and simultaneously serve as an insulator. The thermal insulation is a composite of Al and mylar. In this paper we will deal only with radiation damage to the metallic components of the magnet system. Those problems associated with epoxies, ceramics and organic polymers will be dealt with in a future paper.

In order to predict the performance of any material, the operational environment must be defined. For a typical fusion magnet system those conditions are as follows:[2]

a) 4.2°K or lower
b) Neutron flux of 10^9 n/cm^2 / sec
c) 85 kilogauss
d) stresses around the yield point of copper and 50 ksi in the stainless steel.

With these conditions in mind we can now investigate the characteristic features of neutron irradiation at low temperatures.

II. RADIATION DAMAGE AT LOW TEMPERATURES

The production of radiation damage at low temperatures is not significantly different from high temperature production. In the neutron case, a neutron enters the lattice and can impart a small fraction of its energy, 4/M, to a lattice atom. This lattice atom, referred to as a PKA, careens through the lattice losing energy by ionization and displacing atoms from their equilibrium sites to interstitial positions. Near the end of its travel, the PKA begins to strike atoms every lattice spacing and creates what is known as a displacement spike (Figure 1). Usually accompanying this displacement spike is a large amount of thermal energy or thermal spike. The displacement spike is an important characteristic of neutron irradiation as opposed to electron or heavy charged particle irradiation. The displacement spike segregated the defects: the interstitials in an outter corona surrounding a core of vacancies or the depleted zone.

An important event which we have neglected in the above sequence is the replacement defect. As the energy of a displaced

atom falls below a certain value, usually taken as twice the displacement energy, no further displacements can occur. However, the primary atom may impart most of its energy to the lattice atom which then proceeds on to a subsequent collision. In the process the PKA comes to rest in the vacated lattice site. For pure metals this type of event has little effect but it becomes important for ordered alloys and compounds.

In the above discussion we have neglected the fate of the neutron. Depending on its energy this neutron can enter into nuclear reactions with the lattice atoms changing them to entirely different elements. This form of damage is completely independent of temperature and therefore will not be effected by annealing. We will return to this point later since it is both permanent and accumulative.

What then characterizes low temperature irradiation effects? The sole significant influence of temperature on the observed irradiation changes is the degree of mobility of these defects. In the case of most metals at 4.2°K the thermal mobility of the defect is extremely small. One of the exceptions is Al where a very limited mobility seems to exist at 4.2°K.[20] Nevertheless, the driving force for the mobility of these defects is not entirely temperature dependent. Each defect has associated with itself a stress field which enables it to interact with other defects. Naturally as more defects are produced, these interactions become more numerous and leads to the observed saturation of irradiation induced defects.

As one would expect, the annihilation of defects on annealing at higher temperatures has been the source of extensive investigation. At the lower temperatures the sequence is rather simple. The interstitials having a lower migration energy ($U_m^i \cong .05$ eV) become mobile first. The interstitials may a) recombine with vacancies b) be trapped by impurities, c) be annihilated by dislocations, grain boundaries, etc. or d) combine with other interstitials to form clusters. At higher temperatures the vacancy begins to move and has the same options as the interstitials. The basic pattern of defects resulting from these migrations will determine the annealing pattern at higher temperatures.

With this brief overview of low temperature irradiation let us now consider the effect these defects have on certain specific pure metals and alloys of interest in a superconducting magnet.

III. ANALYSIS OF RADIATION EFFECTS TO PURE METALS AND ALLOYS

While it must be evident from the general introduction, it is important to point out that each material plays a special role and therefore was chosen for a special physical property. Thus, copper and aluminum were chosen for their low resistivity, NbTi for its high critical current and field, and stainless steel for its strength and ductility at low temperatures. All three materials will exhibit different changes in their design properties due to irradiation. However, one characteristic common to all is the energy stored by the defects produced by this low temperature

irradiation which will be released upon annealing. In the following sections all of these aspects will be treated in detail, and applied to the UWCTR.

Resistivity Changes in the Pure Metals Cu and Al

In an analysis of the resistivity changes in copper and aluminum an important parameter to be determined is the rate of change of the resistance with increasing neutron flux. In early work done by Burger et. al.[28] the derivative of resistance with dose was assumed to be linear. An integration with respect to time of $d\rho_r/dt$ yields equation III-1 for ρ_r

$$\rho_r = B\,[\,1 - \exp(-\beta t)\,] \qquad \text{(III-1)}$$

Obviously, this result is not in agreement with the known mobility of the defects due to the stress fields of each defect. In recent work by Horak and Blewitt[5] the recombination volume of the defects are taken into account and the rate of increase of resistance then varies with the square of the flux and yields the following expression III-2.

$$\frac{d\rho_r}{dt} = A\left[1 - \frac{2\alpha_{ro}\rho_r}{\rho_{FP}}\right]^2 \qquad \text{(III-2)}$$

This expression can be extrapolated to two straight lines similar to III-1 where the cross-over point occurs at a neutron flux of 3×10^{15} cm^{-2}. Table 1 and Figures 2 (a and b) given the experiment data points and the constants for expression III-2. Table 2 gives the saturation values for these pure samples.

As we have previously pointed out the energy of the incoming neutrons will have a significant effect on the type of defect produced. It is therefore, necessary to evaluate the effect of neutron spectrum on the resistance changes. For the purposes of this analysis we will divide spectrums into two groups: 1) a predominantly thermal neutron spectrum and 2) a fast neutron spectrum. In the former case we need only to consider the displacements due the recoil nuclei of the (n,Y) reactions. From Table 3 we can see that the energy of the "PKA" is of the order of a fraction of a kev.[9] From this type of a spectrum one would expect defects similar to those resulting from electron irradiation, that is, an absence of displacement spikes. In the fast neutron spectrum the defect structure will be predominantly spikes and clusters. Annealing curves for copper and aluminum are shown in Figure 3 for several flux spectrum.[6] Of notable importance is the absence of effect in the aluminum samples. This insensitivity of Al to spectrum can be explained by its low capture cross section and in general by the increased

importance of ionization effects in light elements. However in the Cu samples the increased annealing at low temperatures can be directly related to the absence of displacement spikes.

In addition to the difference of the type of defect present, the transmutations resulting are significantly different. In general the cross section for (n,γ) is much larger at thermal energies than $(n,2n)$, (n,p) and (n,He_4) at high energies. The contribution from (n,γ) transmutation products to the resistivity increase can be on the order of 10% from Coltman et. al.[9]

The study of irradiation damage recovery from annealing is important from the standpoint of engineering application as well as the understanding of fundamental mechanisms. As a result experimental investigations in this area are numerous.

The annealing recovery process is divided into several stages. Stage I is characterized by the migration of the interstitials which continues up to 60°K for copper and 50°K for aluminum.[19] Within this stage we find five separate substages: the first three (A,B,C) represent close-pair annihilation, and last two (D and E) are characterized by free migration of the interstitials, D corresponding to a small number of steps and E a large number of steps.[20] Figure 4 illustrates these substages for electron irradiated Cu and Al and Figure 5 neutron irradiated samples. Notice the relative size of the A to C peaks between the two types of irradiations indicating the lack of close-pairs in the neutron case. A characteristic of aluminum is the

absence of the A peak indicating a limited mobility of aluminum even at liquid helium temperatures. Of importance to the engineer is the defect retention after stage I annealing shown in Figure 6. This data indicates 65% retention for Cu and 50% retention for Al.[20]

In Stage II (60 to 220°K for Cu and 50 to 170°K for Al) we find no basic change in the pattern. The mean density of the defects is reduced due to elimination of thermally unstable interstitial-vacancy and trapped interstitial structures.

The migration which occurs in Stage III (220°K and up for Cu and 170°K for Al) is still under discussion. The situation is extremely dependant on the structures formed in earlier anneals. For Al a vacancy migration theory is in good agreement with experiment while for Cu the conversion-two-interstitial appears to apply.[20] The free migration of vacancies seems acceptable for Al with its low melting point.

Stage III annealing reveals an important difference between Al and Cu from the engineering standpoint. Recovery is complete for Al at room temperature (Figure 7) whereas defect retention is still 20% for Cu (Figure 8) complete recovery occuring only at temperatures greater than 500°K.[20] One last effect that might be important for UWCTR is the shift of annealing peaks to lower temperatures with increasing fluence. This would be expected since more defects decreases the inter-defect distance and increases the probability of annihilation (Figure 9).

Irradiation Effects to Superconductors

Before one could enter into an examination of the effects of radiation on superconducting properties, it is necessary to understand what this state implies and in what environment it can exist. Some materials at very low temperatures make an abrupt transition to a non-resistive state. This superconducting state is possible within a region below the critical values of temperature, current, and magnetic field which differ for each material. Figure 10 defines this region for Nb_3Sn [3]. The critical temperature T_c can vary up to 21°K, the critical field H_c up to 400 kilogauss, and critical current J_c up to 10^6 amps/cm^2. Unfortunately, we cannot achieve these limits simultaneously. Both T_c and H_c are mainly properties of the material's electronic distribution and are not changed significantly by defects in the lattice. Of the radiation effects to be studied, transmutation reactions could effect T_c and H_c since they introduce new materials changing the electron distributions. The lattice defect contribution to T_c is through the effect of the phonon frequency, but this term generally makes only a small contribution to T_c. However, in some materials, Nb_3Sn for example, ordering plays an important role in T_c and therefore disordering effects due to displacement, and more important, replacements need to be considered. On the other hand, J_c is strongly dependent on the defect structure. In order for a superconductor to carry current, the flux lines

must be pinned by defects to stop their motion under the Lorentz force. However, not all defects are equally effective as pinning sites and therefore the better the defects are at pinning, the higher the attainable J_c. The critical current density is not only proportional to the defect density but also to the degree of difference between the defect and the matrix. This latter condition will become important in our interpretation of the experimental results in the next sections. The role that both defects and precipitates play in increasing J_c can be seen in Figure 11, where J_c verses H curves are shown for various annealing procedures. Annealing at 450°C introduces α-Ti precipitates increasing J_c.[4] Lower annealing temperatures (i.e.200°C) yields precipitates to small to be effective pinning sites while a 650°C anneal produces precipitates too large to be effective and makes significant changes in the matrix alloy composition. The phase diagram for the Nb-Ti system is shown in Figure 12.

Useful superconducting materials basically fall into two metallic types: 1) alloys like NbTi and NbZr and 2) intermetallic compounds like Nb_3Sn, Nb_3Al, V_3Ga and many others. In general the alloys have good ductility and bond easily with copper. The intermetallic compounds, on the other hand, are of the beta tungsten structure, seen in Figure 13, which is the source of higher T_c, H_c, and J_c than for the alloys. However, this structure is extremely brittle and these compounds require complicated fabrication processes in addition to being more expensive. Present day magnets either use NbTi or Nb_3Sn with NbTi predominant for the reasons mentioned above.

Irradiation Studies

As a prelude to an indepth discussion of irradiation effects to superconductors, it is helpful to investigate where research has already been completed in terms of irradiation temperature and fluence dpa (Figure 14).

Since the equilibrium defect structure at 300°K is quite different from that at 4.2°K, over 50% of the data points are not applicable to the fusion reactor case. Although we have several points at 4.2°K, those investigations include only one study of neutrons on NbTi and none of the neutrons on Nb_3Sn. In order to acquire the ability to predict the performance of a superconducting magnet system in a fusion reactor, it would seem that more data is needed in the low temperature region. Nevertheless, we will try to come to some understanding of the effects already brought to light by all these irradiation studies.

NbTi and NbZr Alloys

As we have noted before, the current carrying capacity of a superconductor is due to defect density and the degree of difference between the defect and the matrix. Physical heterogeneities can be introduced into materials by mechanical deformation, second phases precipitation, impurities, or lattice imperfections. For the ductile alloys NbTi and NbZr, second phases and mechanical deformation are the important mechanisms. For the most part, fabrication processes of these alloys and heat treatment depend on deformation/to achieve high critical current densities. It has been found[21,22] that maximum flux pinning is obtained

when the dislocations form a cellular structure referred to as tangles seen for Al in Fig. 15.These tangles or cell walls in niobium are 100-500 °A wide, and the essentially dislocation-free cells have diameters of~0.6 microns. Magnetization studies, illustrated in Figure 16, show that these tangles are much more effective as pinning sites than are single dislocations. Once the cell structure is formed at a dislocation density of 10^9 (15-20% cold work), then additional deformation makes little change on the magnetization or the critical current. These results have been confirmed by many authors.[21]

With this in mind, we can interpret radiation damage studies to NbTi and NbZr. The earliest and perhaps the most complete report of radiation damage at low temperature (30°K) was completed by Coffey et. al.[7,11]. In all cases deuteron irradiation caused a slight increase or no change in the J_c of annealed samples while causing decreases of 25% and more to cold worked NbZr and NbTi (figure 18). Note also the drop in J_c by more than a factor of20 from the cold worked (Figure 18a) to annealed (Figure 18d) samples. In Figures 18c and d we see what is known as the peak effect: a hump in J_c at high fields. It is particularly interesting since it only anneals out at 300°K indicating a defect other than simple point defects. Even today this effect has not yet been satisfactorily explained.

Coffey[11] also determined changes in T_c and H_c for these deuteron irradiated samples. The T_c decreases were small and of the order of -3.3% (-.2°K). However, since H_c depends on T_c in a parabolic manner (Fig. 19), H_c should decrease by 12% which agrees with the experimental evidence.

The only other significant study of low temperature irradiation effects on NbTi has been made recently by Wipf and Soell.[8] Fig. 19 shows the results of their neutron irradiation work but the value of the paper is best seen in their explanations of them. In general, they found decreases in J_c with neutron dosage. There could be three sources for these decreases:

1) A decrease in T_c. Since the critical point for a superconductor is a function of T_c, J_c, and H_c (Fig. 18) simultaneously, a negative change in T_c could conceivably account for the decrease in J_c. However, Wipf points out that this change in T_c must be of the order of several °K to agree with the experimentally determined changes in J_c. Measurements in similar experiments show a $\Delta T_c \approx -0.2$°K[11] and therefore the conclusion is made that this effect is minor for NbTi even though T_c was not measured for these specific samples.

2) Phase transformations and precipitation due to the high temperatures of ionization produced spikes. This effect is ruled out since the effects can be annealed out at a low temperature. It would not be possible if these effects were

due to precipitates. It is further debatable whether destruction of precipates would noticably affect the current carrying capacity of the wire used in this experiment.

3) Reduction of the pinning strength of the dislocation tangles. Figure 20 illustrates the model on which this explanation is based. As we have previously seen, essentially dislocation-free matrix is surrounded by dislocation cell walls which form pseudo-potential wells to flux pinning. During irradiation, point defects have been introduced in the matrix decreasing the degree of difference between the walls and the matrix and, in an explanatory way, decreased the depth of the potential well. This model, of course, assumes that the point defects do not increase the wall pinning effectiveness.[8] Reasons for this assumption are the belief that the high defect density of the walls would suppress the effect of the point defects and, furthermore, that it is possible for the dislocations to act as sinks for the irradiation induced point defects. This model requires substantially more data to be proven but appears to provide a reasonable explanation to J_c degradation.

It is important to note here that the current carrying capacity of a NbTi alloy may be enhanced by two methods: 1) cold working and 2) precipitation heat treatment. The latter method is only possible for Ti rich alloys and is the technique commonly adopted by U.S. producers. On the other hand, the material tested by Wipf and Soell was primarily

of the cold-worked type, and the proposed model is valid. For precipitation heat treated superconductors, another model must be used involving the breakup of precipitates. It is the author's opinion that this second model will show, based on the work of Nelson et. al.,[3] slower dependence on neutron dose and will be more radiation resistant than the alloy dependant solely on dislocation networks for flux pinning.

Intermetallic Beta-Tungsten Compounds (Nb_3Sn, and others).

At its initiation, the interest in irradiation studies of the intermetallic compounds stemmed from a different motivation. As we have noted previously, these compounds are extremely brittle and therefore, enhancement of the critical current could not be obtained by deformation. Initially, the concentration was on methods using second phases and impurities in order to obtain J_c enhancement. However, particle irradiation presents itself as a convenient method of homogeneously introducing lattice defects into the superconductor. The immediate conclusion would be that the effect on J_c should be positive as opposed to the negative effect seen in highly deformed alloys. This is not completely true due to large effects on T_c in some of these materials.

From Table 4 we see that again the work of Coffey et. al.[11] is not only the first but the only irradiation study of any kind on Nb_3Sn systems at cryogenic temperatures ($T < 300^{\circ}K$). The reason is obvious. Defect mobility is required to form

the large defect structures such as clusters, platelets and loops necessary for effective flux pinning. Therefore, higher temperatures are necessary.

Analysis of the work of Coffey et. al.[11] reaffirms some of the conclusions that we have made concerning the alloys. The J_c versus H curves (Fig. 21) derived from their experiments again indicates the difference between initially high J_c (Sample 251) and initially low J_c (Sample 184) Nb_3Sn. In Figure 21a, we see an increase of J_c in 184 due to a small percentage of large thermally stable (T_c 300°K) defect clusters. Figure 21c and 21d show the opposite effect, a net decrease of J_c for 251. However, an investigation of J_c versus H_c curves as a function of temperaure reveals a negative effect at higher fields for both materials due to the decrease in T_c. Remember that in the alloys this effect was negligible. This is not the case for Nb_3Sn which depends on ordering for its high critical temperature. A T_c decrease of 1.2°K (-8%) was measured for these samples and the strong T_c dependance on H_c accounts for the net decrease of J_c at high fields. This decrease was not recovered by annealing at 300°K and would not be recovered until T ~ 1000°C (Fig. 22) where reordering can occur.

From the previous discussion of intermetallics, in general, one can see that any effort to compare different studies could be extremely difficult. Since J_c is a sensitive function of stoichiometry,

slight deviations from 29.5 weight % Sn can change the current carrying capacities drastically, and therefore, the radiation effects differ drastically. In addition, Nb_3Sn is fabricated through many different processes leading to different properties caused by differences in impurities, heat treatments, stoichiometry,etc.

From the works of Cullen, Novak[12-14], and the as yet unpublished work of Bett[15], we can piece together the effect of "high" temperature irradiation on Nb_3Sn and the results are not surprising (Figure 23,24,25). Basically the effect can be separated into two counter-effects: 1) increase J_c by introducing defects, and 2) decrease J_c by introducing disorder, thereby lowering T_c. The fluence at which the decrease of J_c overtakes the increase depends on the initial current carrying capacity of the superconductor (Figure 26a). In order to put Figure 26 into perspective, note that the ordinate represents J_c^{irr}/J_c°. J_c° is not the same for each sample and ranges from 1.36×10^5 to 1.2×10^6 amps/cm^2, lowest to highest respectively. I would anticipate the lowest initial J_c sample to fall off precipitously in the range of 5×10^{18} n/cm^2. The data of Bett (Figure 26b) enables us to see clearly the magnitude of the decrease in T_c.

Annealing Recovery of Superconducting Properties

When a fusion magnet engineer talks of annealing procedures, he is considering a relatively low temperature anneal. The annealing temperature will probably not exceed room temperature by many degrees due to the constituents

of the magnet. This temperature must in no way approach the charring point of the lowest melting material in the magnet (probably the insulation).

In previous studies, we have seen that point defects anneal at temperatures between 77°K and 300°K[11]. In that range of temperatures, we can recover from 85 to 100% of the current carrying capacity depending on the material and the extent of radiation damage.[8, Figure 28] This is particularly true for the metallic alloys. However, when decreases of T_c are significant as in Nb_3Sn, then much higher temperatures must be reached to regain the ordered structure. For Nb_3Sn, even temperatures of 450°C for periods of days yield little recuperation of T_c as seen in Figure 29.

This requirement of annealing temperatures has also been seen through experiments monitoring the lattice expansion. It was found that annealing at 650°C for two hours was sufficient to relax the lattice to the initial size. This temperature is higher than would be expected from a material with a melting point of 2400°K but this is thought to be due to the highly ordered state of Nb_3Sn.

Mechanical Properties of Structural 304 Stainless Steel

The mechanical properties of interest to us, i.e. yield strength, ductility and creep are significantly affected by changes in the dislocation-defect interaction. Irradiation defects may impede the motion of dislocations thus increasing the strength

while decreasing the ductility. Creep is usually associated with vacancy concentration and diffusion. The vacancy concentration is increased during irradiation and may lead to irradiation induced creep even at temperatures where thermally activated diffusion is zero.

While changes in these properties are important to the designer, very little work has been done in this area at cryogenic temperatures. At this time, no work has been done at liquid helium temperatures and no more than four papers have been written on the temperature range of liquid hydrogen and nitrogen.[25,26,27,29] No data has shown statistically reliable changes in the yield strength and ductility of 304 SS, even though decreases in strength were indicated.[25] For $5x10^{16}$ n/cm^2 (E>1.0 MeV), 347SS shows significant decrease (35%) in yield strength with little or no change in ductility.[26] Explanations were not presented in the literature. Type301 exhibited a smaller decrease in yield strength (5%) but no statistical reliability was given.[26,27] In light of the spotty data and the absence of explanations for phenomena already seen, further experiments would seem indicated.

At high temperatures and with energetic neutrons, severe embrittlement has been observed. This is predominantly due to stress at brain boundaries from helium. At temperatures where diffusion of helium and hydrogen cannot take place, the gas remains in the matrix and only slight degradation in properties should occur.

An interesting area of irradiation damage has been the area of creep. Normally, creep is considered to be a thermally activated

process. However, in the last few years, extensive work has been conducted dealing with irradiation induced creep. This subject will be dealt with completely in a later paper and its effect applied to the magnet system design.

Stored Energy Due To Irradiation Defects

In the past, the amount of stored energy in an irradiated material has largely been overlooked as a source of design limitation and in general, this is true. However, operating procedures may be affected if the energy stored reaches values compared to the heat capacity of the material and the thermal heat flux due to thermal conductivity or coolant. In any cryogenic system, the latter term is by design very small and the heat capacity at low temperatures is very small increasing as T^3. It would, therefore, seem wise to analyze this aspect to avoid undesirable runaway heating on warm-up.

Estimates of the energy contained in a Frenkel defect can be made by summing the energy of formation of both the interstitial and the vacancy. This estimate indicates a value of 3.5 eV for copper and 5.6 for aluminum. The product of this energy and the total number of frenkel pair will then indicate the magnitude of the stored energy.

This value is only approximate at best and some experimental work has been done correlating the change in resistance with the energy releases during isochronal annealing. One would expect that the energy stored would be less than the theoretically derived value simply due to thermal spike annealing and recombination. One would

expect the energy released to vary within each stage as is the case for copper. The mean of several experimenters yield 6.7 cal/gm/10^{-6}ohm-cm for stage I Cu and 12.8 for state II and III. For aluminum, all three stages have the value of 8.37 cal/gm/10^{-6}ohm-cm.[30]

We can see from this brief survey of irradiation effects that an incorporation of these time dependent changes into the materials choice of the magnet system is both necessary and complicated. The results can place limits on the initial choice of materials as well as the manner in which the reactor system is operated.

IV. APPLICATION TO UWCTR

The cryogenic magnet design that was adopted for the preliminary CTR presented by the University of Wisconsin at the 1972 Austin Symposium represents a major improvement of past magnet designs.[31] This design, shown in Figure 30, uses the constant tension concept with edge cooling of the superconductor.[1,2,31] The cast stainless steel structural component consists of a large disc in which shallow grooves have been left. These grooves are filled with the conductor which is then epoxied in place. This procedure allows the copper to be prestressed by keeping the stainless steel disc in tension during the application of the epoxy. Prestressing increases the efficiency of the stainless steel.

In this design, use is made of the total stability criterion which states that the cooling capacity of the helium must be greater than the amount of heat generated by the current flowing in the stabilizer.[32] This criterion presupposes that the current is forced to leave the superconductor for one reason or another. The resistance then plays an important role in the criterion and determines the cross section of copper needed in the magnet.

The sources of resistance are numerous and, following Matthiesen's rule, are independent of each other. The total resistance can be represented by a summation of six terms: the residual imperfection resistivity ρ_o, the temperature dependent resistivity $\rho(T)$, the stress induced resistivity ρ_S, the magnetoresistivity ρ_M, the radiation induced resistivity ρ_R, and the impurity induced resistivity ρ_T.

$$\rho = \rho_o + \rho(T) + \rho_S + \rho_M + \rho_R + \rho_T \qquad \text{(IV-1)}$$

Recent work by Lengeler, Schilling, and Wenzl indicates that there may exist coupling between these terms in cold-worked and neutron irradiated copper.[33,34] Nevertheless, in the following work, these deviations will be ignored and the validity of Mattheisen's rule accepted. At 4.2°K, the temperature dependent term is several orders of magnitude less than ρ_o and can be neglected. The magnetoresistivity has been shown to be strongly dependent on ρ_o and has been studied over large ranges of impurity concentrations. The impurity concentration is usually measured in a manner probably unfamilar to that is, in terms of RRR, the residual resistance ratio, defined as the room temperature resistance over the resistance at 4.2°K. This ratio is extremely sensitive not only to impurity concentrations but also to the deformation history of the sample, a big disadvantage to the interpreter.

The copper quality usually proposed for a CTR magnet system is designated as oxygen free high purity copper (OFHC) which has a nominal RRR value of 150 and a residual resistivity of 1.44×10^{-8} ohm-cm. Figure 32a plots the change in ρ_M with increasing magnetic field for copper. An analytical expression of the resulting straight line for RRR = 207 is given in IV-2.[35]

$$\rho_M = .064\ B\rho_o \text{ for B in kilogauss} \qquad \text{(IV-2)}$$

In CTR magnet it is tempting to go to lower resistivity simply by increasing the purity. In Figure 32b, we see that the maximum gain is attained for a RRR of 2000. It has yet to be determined if the cost of this high purity is offset by the savings in both copper and stainless steel.

The case for aluminum is considerably different.[36] A resistance versus magnetic field plot (Figure 33a) reveals a saturation of ρ_M at the low field of 30 kilogauss. This characteristic property of aluminum is perhaps the most important item in a comparison between copper and aluminum. Once again, the impurity dependence of the saturation magnetoresistance is of interest (Figure 33b) and the maximum is attained at RRR = 15,000.

While very little has been done on the stress induced resistivity of copper, there is data available for the stressed state of aluminum.[37] For low strains beyond the yield stress, the increase in resistivity can be taken as linear with ε (Figure 33c). For 99.9999% Al (RRR=2000) and strains less than 0.01, equation IV-3 can be used.[37]

$$\rho_s = 2.35 \times 10^3 \rho_o (\varepsilon - .0033) \qquad \text{(IV-3)}$$

For higher strains, some authors believe IV-4 to hold true:[38]

$$\rho_s = \rho_o [A\varepsilon^{5/4} + B\varepsilon^{-3/4}] \qquad \text{(IV-4)}$$

In Figure 33d, the results of both strain and magnetic field are shown.[39] These results, which show a small increase in ρ with plastic strain, are not in agreement with results of Figure 33c and

the application of Mattheisen's rule. In other work on the correlation of radiation induced resistance and magnetoresistance, similar deviations in Mattheisen's rule are found. The author feels that further investigations are necessary to clarify the situation. Strong coupling could be expected from ρ_o, ρ_S, ρ_M and ρ_R, all of which depend to a high degree on the defect structure of the material. Nevertheless, it is the author's opinion that the application of Mattheisen's rule will be the worst possible case and that deviations will decrease the total resistance increase.

Neutron Flux Characteristics

As we indicated in section III, the type and energy of the incoming particle plays an important role in determining the characteristics of the resulting damage. Any evaluation of the radiation damage in UWCTR must include a discussion of the shield and flux spectrum.

Figure 34 gives a schematic of the proposed radiation shield.[31] The role of both the lead and the stainless steel is the slowing down of the neutrons by means of inelastic scattering. After the slowing down has taken place, thermalization and finally absorption takes place in the carbon and boron respectively. This proposed shield yields a neutron flux of 2.2×10^7 n/cm^{2}sec and a displacement rate of 2.3×10^{-14} dpa/sec for 2.3MW/m^2. The energy attenuation is still undetermined due to the lack of data on secondary gamma emission.

It may be seen from Figure 35 that the neutron energy spectrum

is strongly peaked toward high energies with 16% of the neutrons having an energy greater than 4.3 MeV and 86% of energy greater than 0.1 MeV.[40] This spectrum is drastically different from a reactor spectrum and shows a total absence of a thermal neutron peak due to the large boron absorption cross section in the shield. In order to calculate the damage rate in the magnet, the displacement cross section is necessary and is shown in Figure 36 for niobium.[41] Notice that the displacement cross section resulting from (n,Y) recoil atoms is several orders of magnitude less than the cross section due to elastic and inelastic interactions and, excluding the existence of a large thermal flux, can be considered to be negligible. The energy spectrum of UWCTR justifies this assumption. With this information, estimates of the radiation damage to the magnet system can be made.

Displacement Damage

Using the UWCTR energy spectrum at the magnet and the displacement cross sections for stainless steel and niobium, a displacement rate energy spectrum can be calculated.[40] As can be seen from Figure 37, 42% of the displacements are due to neutrons with energies greater than 3.2 MeV and a relatively insignificant percentage of the displacements (2.4%) arising from neutrons of energy lower than 0.1 MeV. For the UWCTR with a first wall loading of 0.5 MW/m^2, the total displacement rate in the niobium is 5×10^{-15} dpa/sec and 6.9×10^{-15} dpa/sec for stainless steel.

In the following numerical applications, the approximation has been made that the displacement rate in both copper and aluminum is equal to the displacement rate in stainless steel. This assumption is probably valid for copper but considerably less valid for aluminum due to the large mass difference between Al and Fe. The radiation induced resistance has been calculated from the general form given by Horak and Blewitt,[5]

$$\frac{d\rho_r}{dt} = A(1 - B\rho_r)^2 \qquad \text{(IV-5)}$$

The constant A can be written as a product of the displacement rate (dpa/sec)and ρ_{FP} in 10^{-4}ohm·cm per defect. The resistance is obtained by integrating IV-5 and applying the initial condition $\rho_r=0$ at t = 0.

$$\rho_r = \frac{1}{B}\left[\frac{ABt}{ABt + 1}\right] \qquad \text{(IV-6)}$$

In this form the constant 1/B is clearly seen to be the saturation resistivity, i.e. $\rho_r=\rho_\infty$ as $t \to \infty$. Equation IV-6 can be written in a different form by multiplying top and bottom of the term in brackets by $1/B\rho_{FP}$ which is equal to the saturation defect concentration $C_{d\infty}$.

$$\rho_r = \rho_{r\infty}\left[\frac{\sigma_d\phi t}{\sigma_d\phi t + C_{d\infty}}\right] \qquad \text{(IV-7)}$$

The values of $\rho_{r\infty}$ and $C_{d\infty}$ determined by Horak and Blewitt for AL and Cu are found in Table 2 and the displacement rate in the UWCTR magnet has previously been determined. Using these values, the following expressions for irradiation induced resistance are valid for the UWCTR magnet and are plotted in Figure 38 versus t.

$$\rho_r(\text{Cu}) = 3.3 \times 10^{-7} \left(\frac{t}{t + 1.9 \times 10^{11}} \right) \text{ohm·cm} \qquad \text{(IV-8)}$$

$$\rho_r(\text{Al}) = 8 \times 10^{-7} \left(\frac{t}{t + 1.76 \times 10^{11}} \right) \qquad \text{(IV-9)}$$

Table 5 gives the resistance increases for three time periods of interest.

Table 5

Irradiation-induced Resistance for Copper and Aluminum in the UWCTR Magnet System

	RRR	ρ_r 1 yr	ρ_r 5 yrs	ρ_r 20 yrs	
Cu	120	5.5×10^{-11}	2.7×10^{-10}	1.1×10^{-9}	ohm·cm
	2000				
Al	2000	1.44×10^{-10}	7.2×10^{-10}	2.88×10^{-9}	ohm·cm

For the UWCTR a change in resistivity of 10% will arbitrarily be deemed unacceptable and thus defines a critical time. Table 6 shows the results for several types of Cu and Al.

Table 6

Critical Irradiation Times and Maximum Wall Loadings for the UWCTR Magnet System

	RRR	10% ρ_o ohm·cm	C_d critical dpa	Critical time (yrs.)	Maximum Wa Loading fo yr. life(MW
Cu	120	1.44×10^{-9}	5.7×10^{-6}	26.5	.67
Cu	2000	8.2×10^{-11}	3.3×10^{-7}	1.5	.04
Al	2000	10^{-10}	1.5×10^{-7}	.7	.02

* For UWCTR Austin Design

It is important to remember here that room temperature annealing will reduce this ρ_r by 100% for Al and by 80% for Cu. One could foresee the possibility of annealing the magnet every two years for example and therefore increase the maximum wall loading by a factor of 10. Without this possibility the use of high purity aluminum or copper is out of the question . This conclusion is evident from column 4 of Table 6 when cool-down times of two months are taken into account.

In a similar fashion, the displacement rate and the accumulative dpa can be determined using only the displacement cross section of niobium in the calculation. The results for several wall loadings and time intervals are presented in Table 7.

Table 7

Displacement Rate in the Superconductor

First Wall Loading MW/m2	Superconductor Displacement Rate dpa/sec	DPA after 1 year	DPA after 20 years
0.5	0.5×10^{-14}	1.6×10^{-7}	0.32×10^{-5}
3	3×10^{-14}	9.5×10^{-7}	1.9×10^{-5}
10	10×10^{-14}	31×10^{-7}	6.3×10^{-5}

A 10% damage level in terms of dpa can be extracted from the data of Soell and Wipf[8] and Bett[15] (Table 8). The conversion from neutron flux to dpa was made using a typical fission reactor spectrum.

Table 8

Effect of dpa on Superconducting Properties

	Reference	-10% Jc dpa	-10% Tc dpa	Change after 3.2×10^{-6} dpa (20 years UWCTR) ΔJc	ΔTc
NbTi	8	5×10^{-3}	x	<0.1%	0
Nb_3Sn	15	4×10^{-4}	6×10^{-3}	~0.1%	<0.1%

As a final displacement damage effect, the stored energy of the defects can be calculated. A dpa value of 5.7×10^{-6} corresponding to the maximum defect concentration allowable for OFHC copper(Table 6) and an average value of 5 ev per defect pair were used in the calculation. A stored energy density of 49 millijoules/gram was determined and compared to the heat capacity of stainless steel which has a value of 200 millijoules/gram/^{o}K at 77^{o}K and 7 millijoules/gram$\cdot^{o}$K at 20^{o}K. It is evident that no significant temperature rise or thermal runaway can occur since significant annealing recovery only begins at 30^{o}K with more than 60% of the energy remaining in the structure at 77^{o}K (Figure 8).

Transmutation Effects

Due to the predominance of high energy neutrons, it was speculated that transmutations might play an important role in the magnet properties (i.e. T_c and ρ). Only transmutations for Nbwere considered for this work because reliable high energy charged particle cross sections are not available for the alloying elements. Table 9 gives the Zr production rates from the (n,α) and (n,p) reactions.

Table 9

Zirconium Production in the UWCTR Superconductor

Wall Loading MW/m^2	appm sec^{-1}	appm after 1 yr.	appm after 20 yrs.
0.5	0.17×10^{-13}	0.54×10^{-6}	0.000011
3	1.0×10^{-13}	3.2×10^{-6}	0.000065
10	3.4×10^{-13}	11×10^{-6}	0.00022

It can be seen from this table that for all conceivable cases, Zr production in Nb will not be a problem in the current design. The same conclusion will probably hold true for the alloying elements, Ti and Sn, as well as for Al, Cu, and 304 SS. In order to become significant, the transmutation products would certainly have to equal the initial impurity concentration of no better than 1 ppm. That represents an increase of roughly four orders of magnitude which seems unlikely at the present time. These conclusions have been substantiated by McCracken and Blow.[42]

V. CONCLUSIONS

In the previous sections an attempt has been made to evaluate the presently available data on irradiation damage to the metallic components of a superconducting magnet. Using this work the following conclusions can be drawn as to the effect of neutron irradiation on the performance of the UWCTR magnet system.

1) Normal Stabilizer: In the present design a 26 year lifetime can be obtained using OFHC copper with a first wall loading of .5 Mw/m^2. It is more resonable to assume that a room temperature anneal can be accomplished at two year intervals and thus the wall loading could be increased to 6.5 Mw/m^2. In the case of high purity stabilizer, this 10% change criterion is extremely difficult, if not impossible, to attain. This latter case would require either an annealing period at less than one year intervals or better shields.

2) Superconductor: For both NbTi and Nb_3Sn the damage is insignificant (<<1% change in J_c and T_c). A comparison between NbTi and Nb_3Sn would seem to indicate that the latter is the most sensitive to irradiation damage. This sensitivity is a result of the disorder which neutron irradiation causes which is detected by the severe reduction of T_c. It is worthwhile to point out that Nb_3Sn has not been studied after neutron irradiation at 4.2°K.

3) Structure: From the meager and inconclusive data, one would expect little change in yield strength or ductility in 304 SS.

In a study such as this, it is hoped that, in addition to predicting the changes to be expected, one would point out where further experimental investigations are needed. With this purpose in mind, the author would like to indicate three areas in which experiments would be beneficial:

1) the deviations from Mattheisen's rule for ρ_o, ρ_S, ρ_M and ρ_R of copper and aluminum,

2) the superconducting properties of Nb_3Sn after neutron irradiation at low temperatures,

3) the mechanical properties of 304 SS at liquid helium temperatures, after neutron irradiation.

BIBLIOGRAPHY

1) H. Desportes, D. Jones and J. Purcell, "Superconducting Magnet for the 15 Foot N.A.L. Bubble Chamber", ANL-HEP-7215 (1970)

2) W. C. Young and R. W. Boom, "Materials and Cost Analysis of Constant Tension Magnet Windings for Tokamak Reactors," Fourth Intern. Magnet Conf., Brookhaven (1972)

3) L. J. Vieland, RCA Rev., 25,366(1964)

4) J. B. Vetrano and R. W. Boom,"A High Critical Current Superconduction Ti-Nb Alloy," Atomics International Report (1964)

5) J. A. Horak and T. H. Blewitt, "Fast Neutron Irradiation Induced Resistivity in Metals," Phy. Stat. Sol., 9 ,721(1972)

6) R. R. Coltman, C. E. Klabunde, D. L. McDonald and J. K. Redman, "Reactor Damage in Pure Metals," J. App. Phy., 33, 3509(1962)

7) E. I. Keller, H. T. Coffey, A. Patterson and S. H. Autler, "Radiation-Induced Peak Effect in Superconducting NbZr," App. Phy. Letters, 9, 270, (1966)

8) M. Soell and S. L. Wipf, "Change in Critical Current of Superconducting NbTi by Neutron Irradiation," Applied Superconductivity Conf., Annapolis, 1972

9) R. R. Coltman, C. E. Klabunde and J. K. Redman, "Survey of Thermal Neutron Damage in Pure Metals," Phys. Rev., 156, 715(1967)

10) T. G. Nilan and A. V. Grante, "Stored Energy Release Below 80°K in Deuteron Irradiated Copper," Phys. Rev., 137, A1233(1965)

11) H. T. Coffey, E. L. Keller, A. Patterson, and S. H. Autler, "Effect of Low-Temperature Deuteron Irradiation on Some Type II Superconductors," Phys. Rev. 155, 355(1967)

12) G. W. Cullen and R. L. Novak, "Effect of Fast Neutron Induced Defects on the Current Carrying Behavior of Superconducting Nb_3Sn," Appl. Phys. Letters, 4, 147 (1964)

13) G. W. Cullen, R. L. Novak and J. P. McEvoy," Effect of Neutron Induced Defects on the Current Carrying Behavior of Nb_3Sn" RCA Rev., 25, 479(1964)

14) G. W. Cullen and R. L. Novak, "Effect of Neutron Induced Defects on the Current Carrying Behavior of Nb_3Sn," J. Appl. Phys., 37, 3348(1966)

15) R. Bett, AERE Harwell (private communication) (1972)

16) B. Lengeler, W. Schilling, H. Wenzl, "Deviation from Matthiesens' Rule and Longitudinal Magnetoresistance in Cold-Worked and Neutron-Irradiated Copper," J. Low Temp. Phy., 2, 237(1970)

17) P. S. Swartz, H. R. Hart, R. L. Fleischer, "Effect of Fast-Neutron Irradiation on Magnetic Properties and Critical Temperature of Some Type II Superconductors," Appl. Phys. Letters, 4, 71(1964)

18) J. P. McEvoy, R. F. Decell and R. L. Novak, "Effect of Neutron Irradiation on Critical Currents in Hard Superconductors," Appl. Phys. Letters, 4,43(1964)

19) J. A. Corbett, "Electron Radiation Damage in Semiconductors and Metals," Solid State Physics, Advances in Research and Applications, Vol. 7 (1966)

20) W. Schilling, G. Burger, K. Isebeck, and H. Wenzl, "Annealing States in the Electrical Resistivity of Irradiated FCC Metals," Vacancies and Interstitials in Metals, edited by A. Seeger, D. Schumacher, W. Schilling and J. Diehl (Wiley, New York, 1970)

21) A. V. Narlikar and D. Dew-Hughes, "Effect of Dislocation Configuration on the Superconducting Properties of Nb and V," Phys. Stat. Sol., 6, 383(1964)

22) R. P. Tucker and S. M. Ohr, "Direct Observation of Neutron Irradiation Damage in Niobium," Phil. Mag., 16, 643(1967)

23) A. Echarri and M. Spadoni, "Superconducting Nb_3Sn: A Review," Cryogenics, August 1971, 274

24) J. F. Kirchner and R. W. Bowman, Effects of Radiation on Materials and Components, (Reinhold, New York, 1964)

25) C. A. Schwanbeck, "Effect of Nuclear Radiation on Materials at Cryogenic Temperatures," Final Report N66-24695 (Jan. 1965)

26) J. J. Lombardo, C. E. Dixon and J. A. Begley, "Cryogenic Radiation Effect on Nerva Structural Materials," The Effects of Radiation on Structural Metals, ASTM-STP 426 (1967)

27) S. H. Bush and J. C. Tobin, "The Effects of Neutron Exposure and Reactor Environments on Stainless Steels," Advances in the Technology of Stainless Steels and Related Alloys, ASTM-STP 369 (1963)

28) G. Burger, H. Meissner and W. Schilling," Analysis of Radiation Annealing Observed During Low Temperature Irradiation with Neutrons and Heavy Charged Particles," Phys. Stat. Sol., 4, 281, (1964)

29) J. C. Wilson and R. G. Berggren, "Effects of Neutron Irradiation in Steel," ASTM Proc., p. 689 (1955)

30) H. Wenzl, "Physical Properties of Point Defects in Cubic Metals," Vacancies and Interstitials in Metals, edited by A. Seeger, D. Schumacher, W. Schilling and J. Diehl (Wiley, New York) 1970

31) M. A. Abdou et. al., "Preliminary Conceptual Design of a Tokamak Reactor," to be published in proceedings of Texas Symposium on the Technology of Controlled Thermonuclear Fusion Experiments and the Engineering Aspects of Fusion Reactors, Austin 1972

32) Z. J. J. Stekly, R. Thome, and B. Strauss, "Principles of Stability in Cooled Superconducting Magnets," Proc. of 1968 Summer Study on Superconducting Devices and Accelerators, Brookhaven, BNL501-55(C-55), 748

33) B. Lengeler, W. Schilling and H. Wenzl, "Deviations from Matthiessen's Rule and Longitudinal Magnetoresistance in Copper," J. Low Temp. Phys., 2 59(1970)

34) B. Lengeler, W. Schilling and H. Wenzl, "Deviation from Matthiesen's Rule and Longitudinal Magnetoresistance in Cold-Worked and Neutron Irradiated Copper" J. Low Temp. Phys., 2, 237 (1970)

35) F. R. Fickett, "A Preliminary Investigation of the Behavior of High Purity Copper in High Magnetic Fields," Annual Report INCRA Project No. 186, June 1972

36) F. R. Fickett, "Magnetoresistivity of Copper and Aluminum at Cryogenic Temperatures," Fourth Int. Magnet Conf., Brookhaven 1972

37) F. P. Ottenmeyer, H. G. Bratsberg, G. M. Graham and A. C. Hollis-Hallett, "The Effect of Strain on the Residual Resistivity of Aluminum," Can. J. of Phys., 42, 1007 (1964)

38) H. G. Van Bueren, Imperfection in Crystals, North Holland Publishing Co., (Amsterdam 1960) p. 155

39) R. Stevenson, "Resistance and Transverse Magnetoresistance of High Purity Aluminum," Can. J. Phys., 45, 4115 (1967)

40) P. Sanger "Radiation Effects in Wisconsin Toroidal Fusion Reactor (WTFR) Magnet Superconductors," FDM 34, University of Wisconsin Fusion Design Team, (1972)

41) D. G. Doran and G. L. Kulcinski (unpublished)

42) G. M. McCracken and S. Blow, "The Shielding of Superconducting Magnets in a Fusion Reactor," UKAEA Report CLM-R120 (1972).

43) R.S. Nelson, J.A. Hudson, D.J. Mazey, "The Stability of Precipitates in an Irradiation Environment," J. Nucl. Mat, 44, 318 (1972).

LIST OF FIGURES

Figure 17 Deleted

Figure 18 Critical current versus magnetic field for deuteron irradiated NbZr and NbTi [7,11]

Figure 19 Stability mapping for a superconductor indicating that changes in J_c, H_c and/or T_c can cause the material to go normal

Figure 20 Critical current versus magnetic field for fast neutron irradiated NbTi; Diagram of the effective defect density for flux pinning across a cell [8]

Figure 21 Critical current versus magnetic field for deuteron irradiated Nb_3Sn [11]

Figure 22 The phase diagram for Nb_3Sn [3]

Figure 23 Experimental results of fast neutron irradiation on the critical current density [14] of Nb_3Sn

Figure 24 Critical current versus magnetic field for high neutron irradiated Nb_3Sn [15]

Figure 25 Critical current versus magnetic field for high neutron irradiated Nb_3Sn [15]

Figure 26a Critical current density versus dpa for Nb_3Sn [15]

Figure 26b Change in the critical temperature due to displacement damage [data replotted from 15]

Figure 27 Critical temperature changes due to high neutron fluences [15]

Figure 28 Effect of annealing on the recovery of irradiation lost critical current [8] of NbTi

Figure 29 Effect of annealing on the recovery of irradiation lost critical temperature of Nb_3Sn [15]

Figure 30a Toroidal magnet cross section with dimensions given for the UWCTR [2]

Figure 30b Various magnet conductor cross sections [2]

Figure 31 Schematic of structural disc for use in UWCTR magnet system [2]

Figure 32a Magnetoresistance of copper versus magnetic field for several values of RRR [35]

Figure 32b Magnetoresistivity of copper as a function of purity [35]

Figure 33a,b Magnetoresistivity of aluminum versus magnetic field (a) and purity (b) [36]

Figure 33c,d Resistance of 99.9999% pure aluminum versus strain [37]

Figure 33d Deviations from Mattheisen's rule for stress-induced magnetoresistivity [39]

Figure 34 Schematic of the blanket and shield of UWCTR [2]

Figure 35 Energy spectrum of the maximum neutron flux to the magnet 300.7 cm from the center of the plasma in WTFR. The total flux at 300.7 cm is 2.16×10^{7} n/cm^2/sec (E < 0.025 eV) normalized to a first wall flux of 10^{14} (2.26 MW/ m^2)

Figure 36 Displacement cross sections for niobium from elastic, inelsatic and absorption reactions [41]

Figure 37 Displacement rate in inner magnet superconductor of WTFR given as a function of lethargy (E_o = 14.9 MeV) the total displacement rate is 2.3×10^{-14} displacements/sec normalized to a first wall flux of 10^{14} n/cm^2/sec (2.26 MW/m^2) The arrows associated with the percent displacement indicates the damage occurring above or below that energy.

Figure 38 Irradiation induced resistance increase in UWCTR (Austin design) as function of fluence for Cu and Al

LIST OF TABLES

Table 1

Recombination volumes for neutron-irradiated metals

element	a) ν_r	b) ν_{r0}	c) ν_r	d) ν_r	e) ν_r	f) ν_r	g) ν_r
1	2	3	4	5	6	7	8
aluminum	416	468	300	300	400	220	280 to 400
copper	400	442	300	300	370	320	490 to 700
silver	438	432	360	260	310	×	425 to 605
gold	274	286	135	190	190	250	270 to 385
platinum	237	255	180	× *)	180	×	×
iron	54	67	43	× *)	×	×	×
nickel	250	284	220	150	230	×	320 to 455
cobalt	300	418	190	×	×	×	×
molybdenum	141	155	120	×	×	×	×

All values given in atomic volumes.
a) Least squares fit of our data to $d\varrho_i/dt = A\,(1 - 2\,\nu_r\,\varrho_i/\varrho_{FP})$.
b) Least squares fit of our data to $d\varrho_i/dt = B\,(1 - 2\,\nu_{r0}\,\varrho_i/\varrho_{FP})^2$.
c) Calculated from $\nu_r = \varrho_{FP}/2\,\varrho_s f$. d) From reference [2].
e) Calculated by the authors using the data of reference [2].
f) From reference [15]. g) From reference [16].
*) No information presented by these authors.

Table 2

Saturation resistivities and defect concentrations for neutron-irradiated metals

element	saturation resistivity ϱ_s ($\mu\Omega$cm)		saturation defect concentration C_s (10^{-3} at. fr.)		resistivity per Frenkel pair ϱ_{FP} (10^{-4} Ωcm/at. fr.)
	present work	Burger et al. [2]	present work	Burger et al. [2]	
aluminum	0.80	0.86	1.2	1.3	6.8 [2]
copper	0.33	0.34	1.3	1.4	2.5 [2]
silver	0.31	0.40	1.2	1.6	2.5 [2]
gold	0.82	0.65	3.3	2.6	2.5 [2]
platinum	1.82	2.1	2.4	×	7.5 [14]
iron	9.23	×	7.4	×	12.5 [13]
nickel	1.14	1.42	1.8	2.2	6.4 [2]
cobalt	2.11	× *)	2.1	× *)	10 (estimate)
molybdenum	3.83	× *)	3.8	× *)	10 (estimate)

Table 3

TABLE IV. New and old values of $\bar{E}_T$ (eV).

Element	$\bar{E}_T$ (new)	$\bar{E}_T$ (old)
Ag	136	124
Au	65.3	81
Cd	129	131
Co	362	305
Cu	374	382
In	86.5	83
Mo	160	149
Ni	525	567
Pd	125	
Pt	70.2	57
Re	38.7	55
Rh	113	88
W	58.3	61
Zn	209	295

7) E.I.Keller, H.T.Coffey, A. Patterson and S.H.Autler, "Radiation-Induced Peak Effect in Superconducting NbZr", App. Phy. Letters, 9, 270, (1966)

8) M.Soell and S.L.Wipf, "Change in Critical Current of Superconducting NbTi by Neutron Irradiation", Applied Superconductivity Conf.,Annapolis,1972

9) W.V. Hassenzahl, J.D.Rogers,H.L.Laquer, W.C. Armstrong, "Radiation Damage in NbTi Superconducting Wires", Third Intern. Conf. on Magnet Technology, Hamburg 1970

10) D.G.Schweitzer, D. Parkin,M.Garber,A.Goland, "Low Temperature Electron Irradiation of Multifilament Superconductors", Applied Superconductivity Conf. Annapolis 1972

11) H.T.Coffey, E.L.Keller, A.Patterson, and S.H.Autler, "Effect of Low-Temperature Deuteron Irradiation on Some Type II Superconductors",Phys.Rev, 155; 355(1967)

14) G.W.Cullen and R.L.Novak,"Effect of Neutron Induced Defects on the Current Carrying Behavior of Nb_3Sn",J.Appl.Phys., 37, 3348(1966)

15) R.Bett, AERE Harwell (unpublished private communication) (1972)

16) H.J.Bode and K.Wohlleben,"Enhancement of J_c in Nb_3Sn Diffusion Layers Produced by Irradiation with Protons",Phys.Letters, 24A,25(1967)

17) F.S.Swartz,H.R.Hart,R.L.Fleischer,"Effect of Fast-Neutron Irradiation on Magnetic Properties and Critical Temperature of Some Type II superconductors",Appl.Phys.Letters, 4,71(1964)

18) J.P.McEvoy,R.F.Decell and R.L.Novak,"Effect of Neutron Irradiation on Critical Currents in Hard Superconductors",Appl. Phys.Letters,4,43(1964)

19) R.Babcock and H.Rickmersma,"Operation of a Superconducting Solenoid in a 440 Mev Proton Flux",Appl.Phys.Letters, 1, 43,(1962)

20) K.Shamoto,T.H.Blewitt, J.E.Brooks and C.Laverick,"Effect of Fast Neutron Irradiation at Low Temperature on NbZr Coil Performance", IEEE Trans. on Nuc. Sci., NS14,No3, 333(1967)

TABLE 40

Ref.	Material	Irradiation Temperature °K	Flux	Particle Energy	Fluence	Change in J_c	σ_1
			Neutron				
18	NbZr	4.2	1.2×10^{9}	8 Mev neutron	4×10^{12}	+.5%	$\sim10^{-4}$
			7.0×10^{9}	fast neutron	7×10^{17}	+2.5%	5.2×10^{-3}
8	NbTi	5	1.5×10^{13}	fast neutron	7.5×10^{18}	-50%	7×10^{-3}
					4.5×10^{18}	-10to15%	6×10^{-3}
17	Nb_3Sn	300	--	fast neutron	10^{18}	positive increase	4.3×10^{-4}
14	"	350	--	fast neutron	6.6×10^{17}	+100%	2×10^{-5}
13	"	350	--	fast nautron	1.4×10^{18}	+125%	6.3×10^{-4}
13	"	370	--	fast neutron	9×10^{17}	-10%	4.1×10^{-4}
					9×10^{18}	-25%	4.1×10^{-3}
					10^{20}	-50%	4.5×10^{-3}
			CHARGED PARTICLES				
7	NbZr	30	--	15Mev deuteron	10^{17}	-5.3	
					10^{21}	-20%to25%	2σ
19	"	4.2	9×10^{6}	440 Mev proton	8×10^{10}	None reported	None
9	NbTi	4.2		13 Mev proton	1.5×10^{17}	None reported	2×10^{-3}
10	"	3	--	1 Mev electron	10^{19}	approximately none	7×10^{-5}
11		30	--	15 Mev deuteron	10^{21}	-10%	2σ
"	Nb_3Sn	"	--	"	"	+100% low J_c	2σ
						-30% high J_c	
16	"	400-600	--	3 Mev proton	$10^{15}-10^{17}$	+400%-max	4×10^{-3}

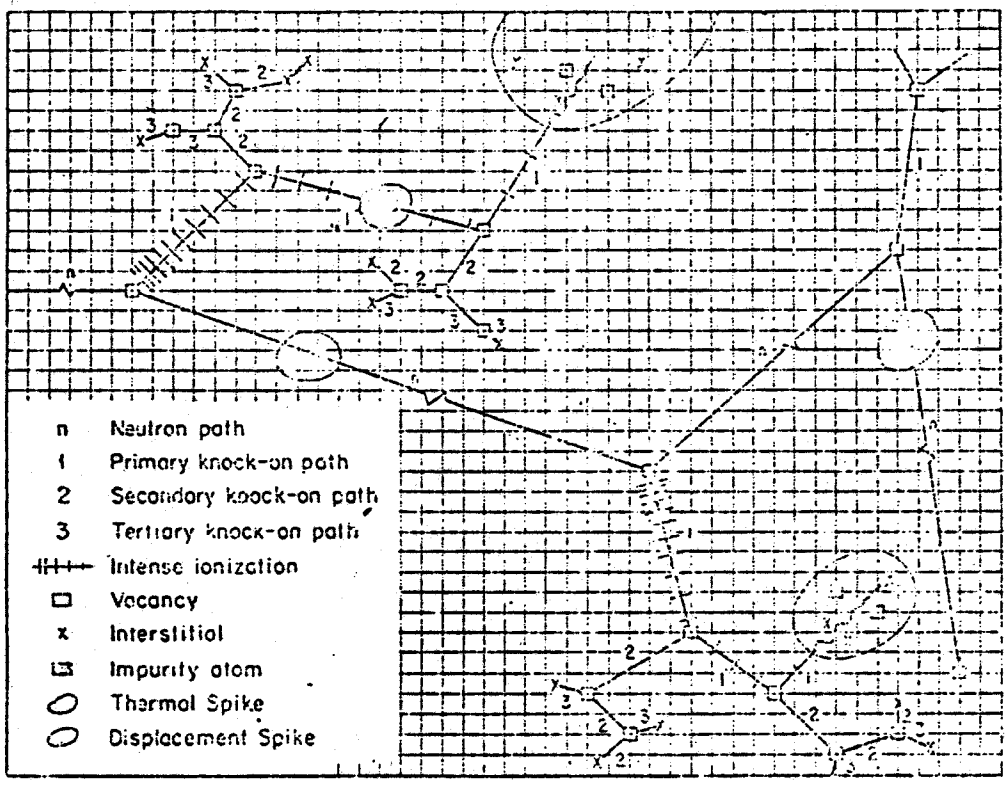

22-2 Radiation effects in a crystal lattice arising from the neutrons entering at the left. (C. O. Smith, *Nuclear Reactor Materials*. Reading, Mass.: Addison-Wesley, 1967, p. 67.)

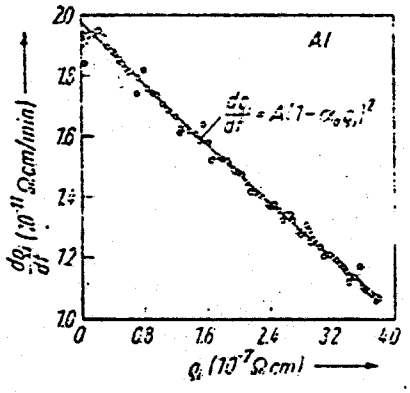

Fig. 2. Irradiation induced resistivity rate, $d\varrho_i/dt$, as a function of induced resistivity, ϱ_i, for Al

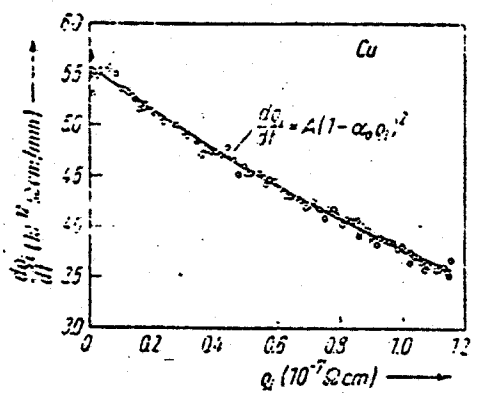

Fig. 3. Irradiation induced resistivity rate, $d\varrho_i/dt$, as a function of induced resistivity, ϱ_i, for Cu

FIGURE 2

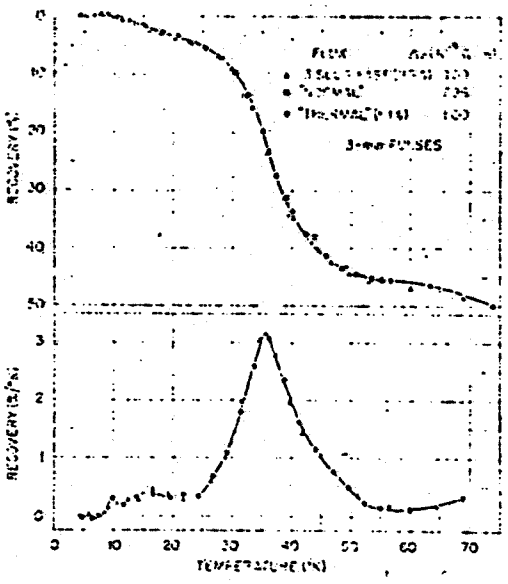

FIG. 5. Isochronal annealing of irradiated aluminum.

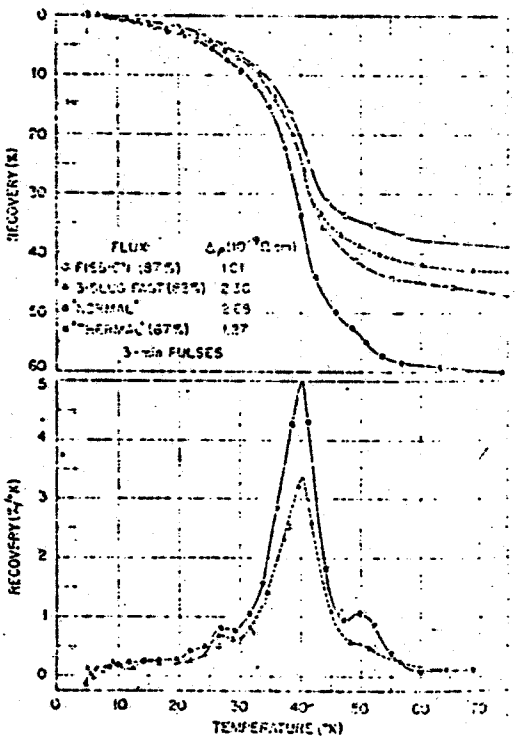

FIG. 6. Isochronal annealing of irradiated copper.

FIGURE 3

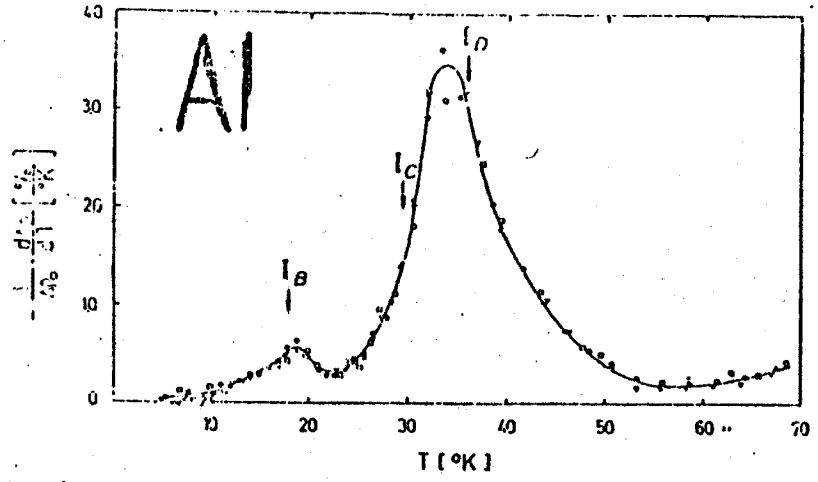

Differential isochronal recovery in stage I of Al neutron irradiated at 4.5°K. The different data points pertain to different independent irradiation and annealing runs. All samples contained about equal initial defect densities $\Delta\rho_0 = 6.0$ nΩ·cm. A smooth curve averaging the results of the different runs has been drawn through the data points. The peak temperatures of the substages observed after electron damage are outlined by arrows for comparison. Data are taken from ref. [57].

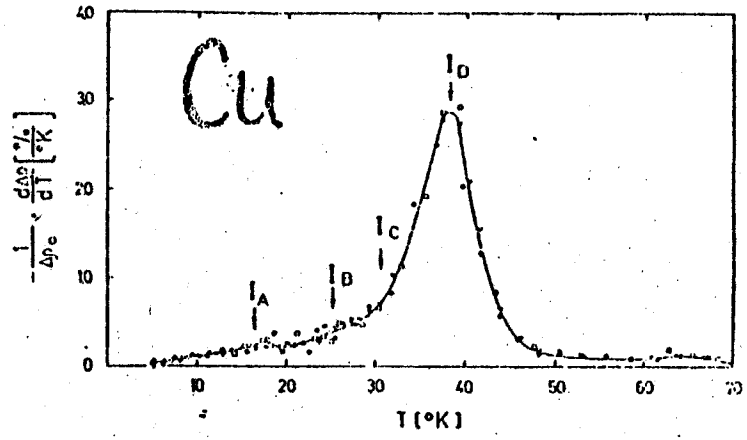

Differential isochronal recovery in stage I of Cu neutron irradiated at 4.5°K. The different data points pertain to different independent irradiation and annealing runs. All samples contained about equal initial defect densities, $\Delta\rho_0 \approx 2.0$ nΩ·cm. A smooth curve averaging the results of the different runs has been drawn through the data points. The peak temperatures of the substages observed after electron damage are outlined by arrows for comparison. Data are taken from ref. [57].

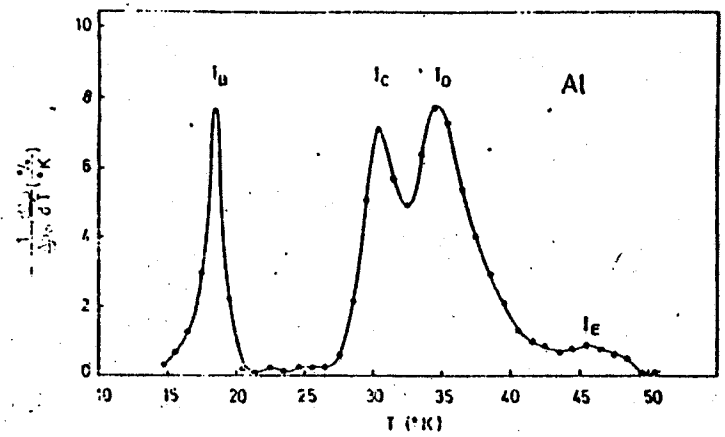

Stage I recovery spectrum of Al after low temperature irradiation with 0.4 MeV electrons to $\Delta\rho_0 = 0.384$ nΩ·cm. Data are taken from ref. [21].

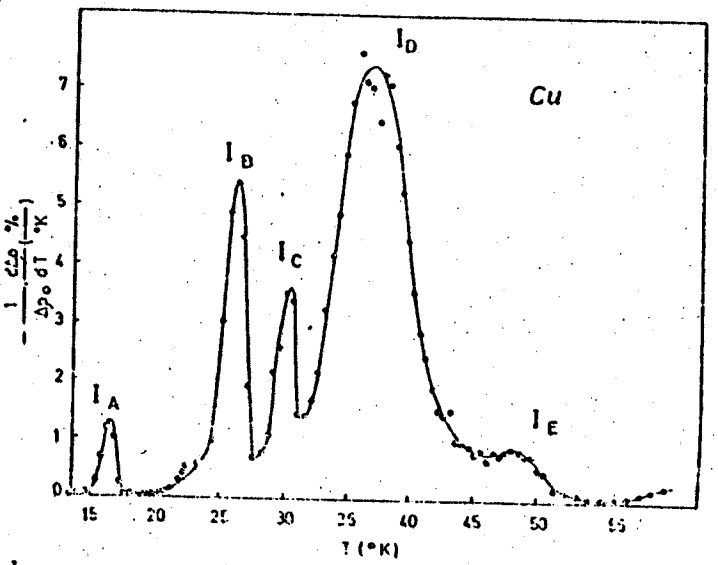

Stage I recovery spectrum of Cu after low temperature irradiation with 2 MeV electrons to $\Delta\rho_0 = 0.134$ nΩ·cm (1 nΩ·cm = 10^{-2} Ω·cm). The data are taken from ref. [15]. A smooth curve which reflects possible fine structure has been drawn through the published data points.

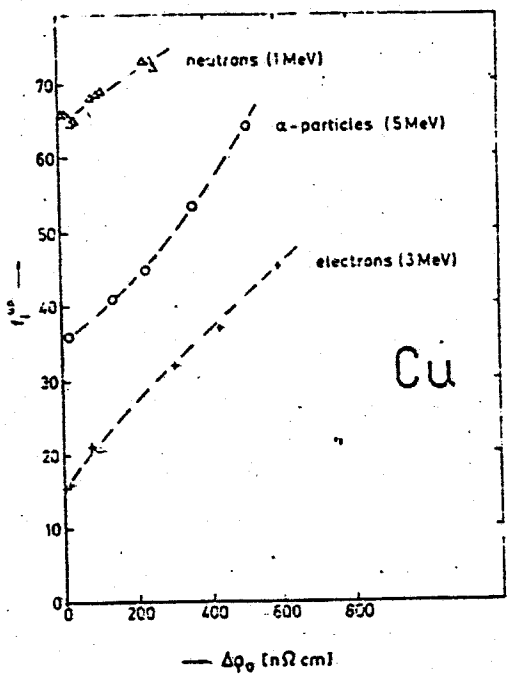

Fig. 32. Fractional defect retention $f_I^{u.p.}$ above stage I (at 60°K) versus defect density $\Delta\rho_0$ introduced by irradiation with different particles in undoped, pure Cu at temperatures below 10°K. Data for neutron, α-particle and electron irradiation were taken from refs. [74,73,36], respectively.

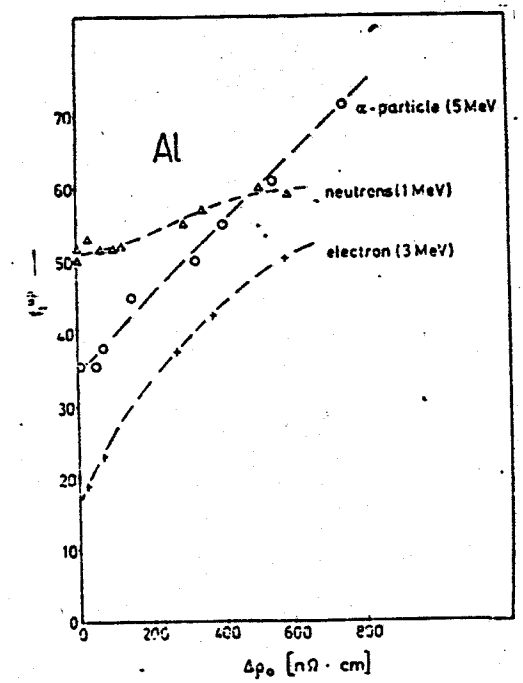

Fig. 33. Fractional defect retention $f_I^{u.p.}$ above stage I (at 60°K) in undoped, pure Al versus defect density $\Delta\rho_0$ introduced by irradiation at 4.5°K (electrons, neutrons) and 20°K (α-particles). Data for neutron, α-particle and electron irradiation are taken from refs. [74,69,36], respectively.

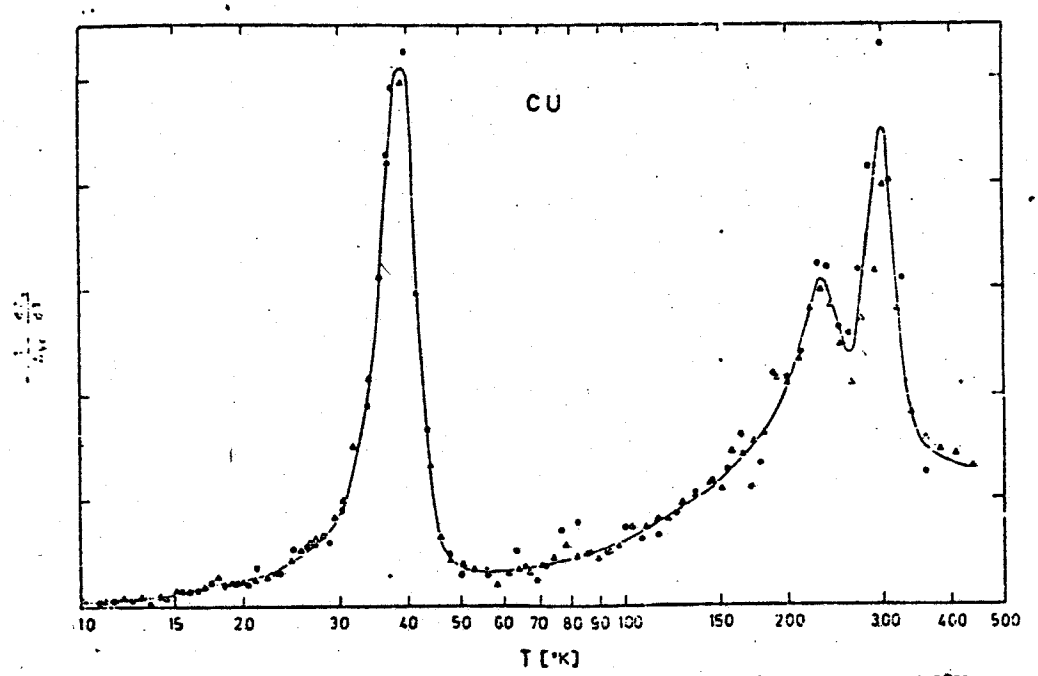

Fig. 42. Differential isochronal recovery spectrum of Cu irradiated with fast neutrons at 4.5°K to $\Delta\rho_0 \approx 2$ nΩ·cm. A smooth curve which averages the results of two independent irradiation and annealing runs has been drawn through the data points. Data are taken from ref. [58].

FIGURE 8

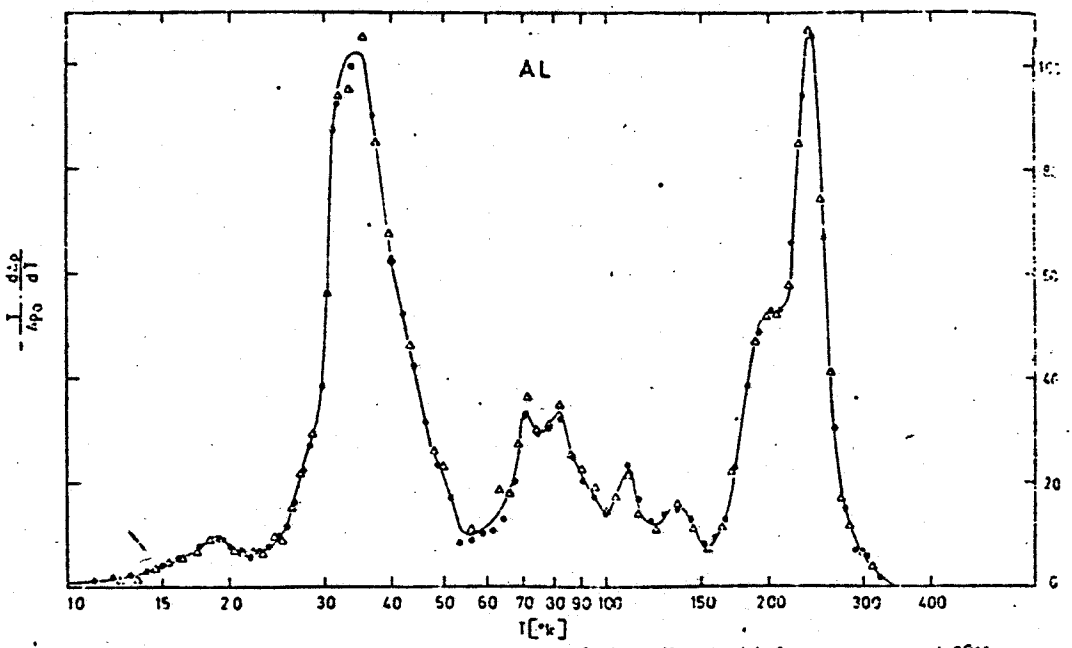

Fig. 44. Differential isochronal recovery spectrum of Al irradiated with fast neutrons at 4.5°K to $\Delta\rho_0 \approx 6$ nΩ·cm. A smooth curve which averages the results of two independent irradiation and annealing runs has been drawn through the data points. Data are taken from ref. [58].

FIGURE 7

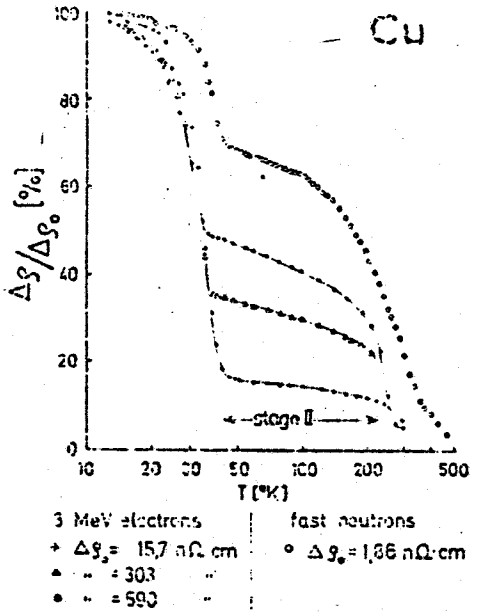

Fig. 39

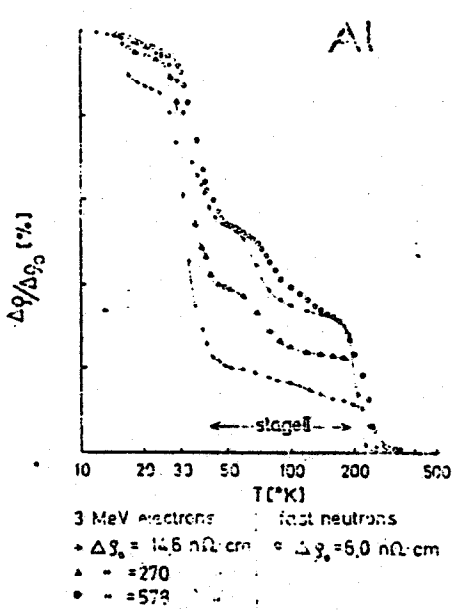

Fig. 40

FIGURE 8b

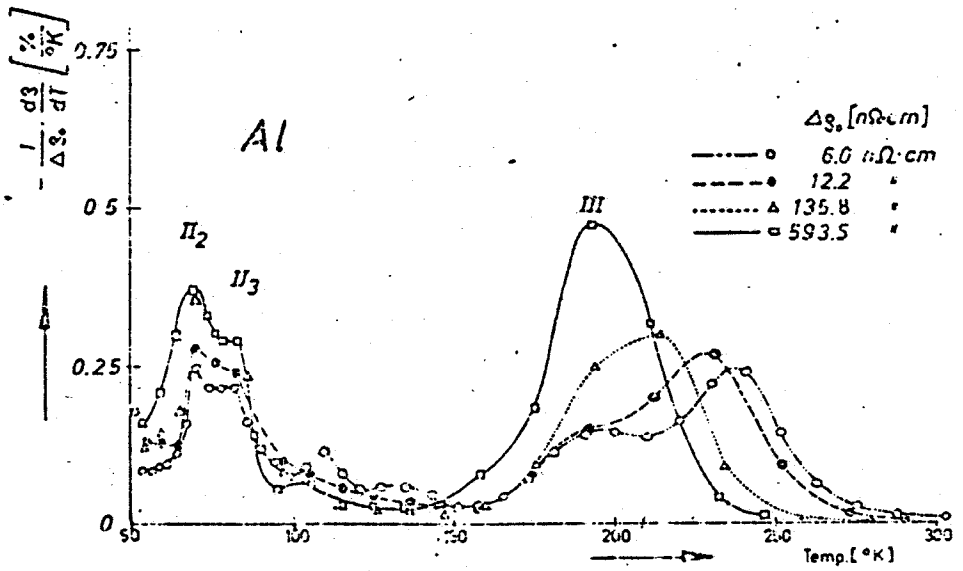

Fig. 49. Dose dependence of the isochronal recovery in Al irradiated with fast neutrons at 4.5°K to the indicated resistivity changes $\Delta\rho_0$. Data are taken from ref. [57].

FIGURE 9

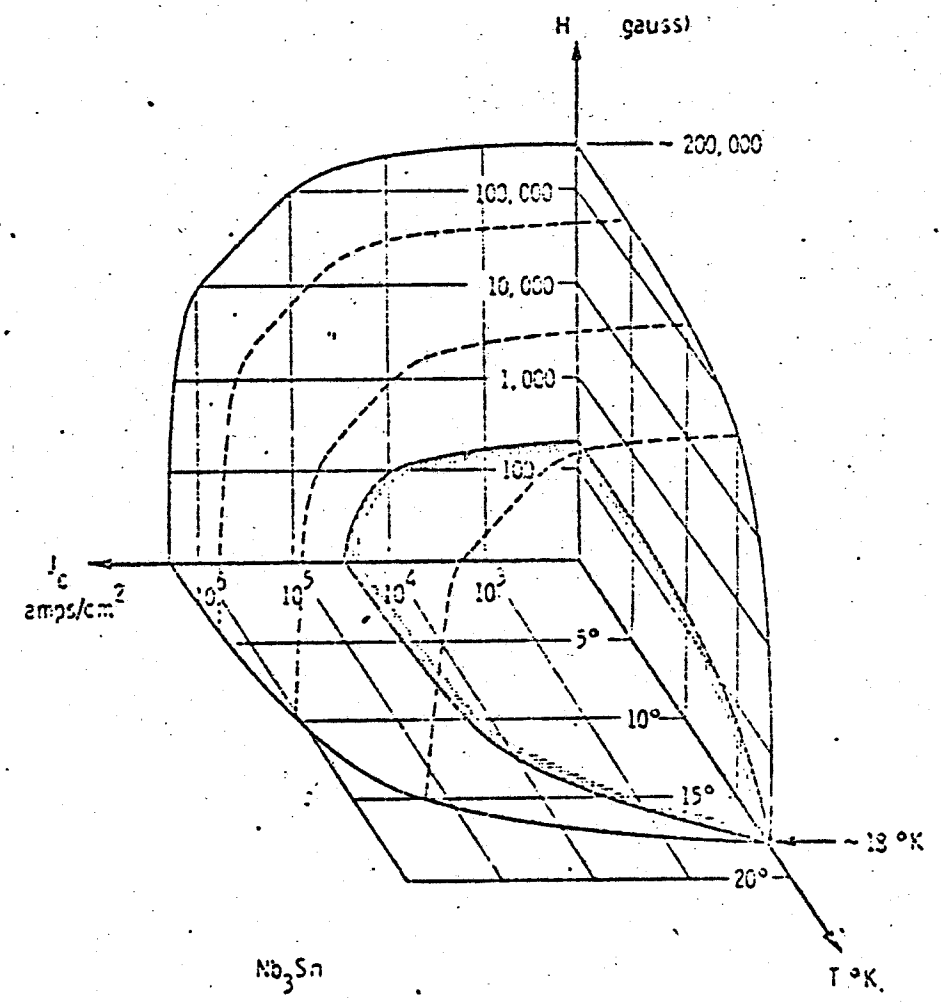

Critical surfaces of magnetic field, current density and temperature for superconducting Nb_3Sn. Type I behavior occurs beneath the inner (shaded) surface and Type II behavior between the inner and outer surfaces.

FIGURE 10

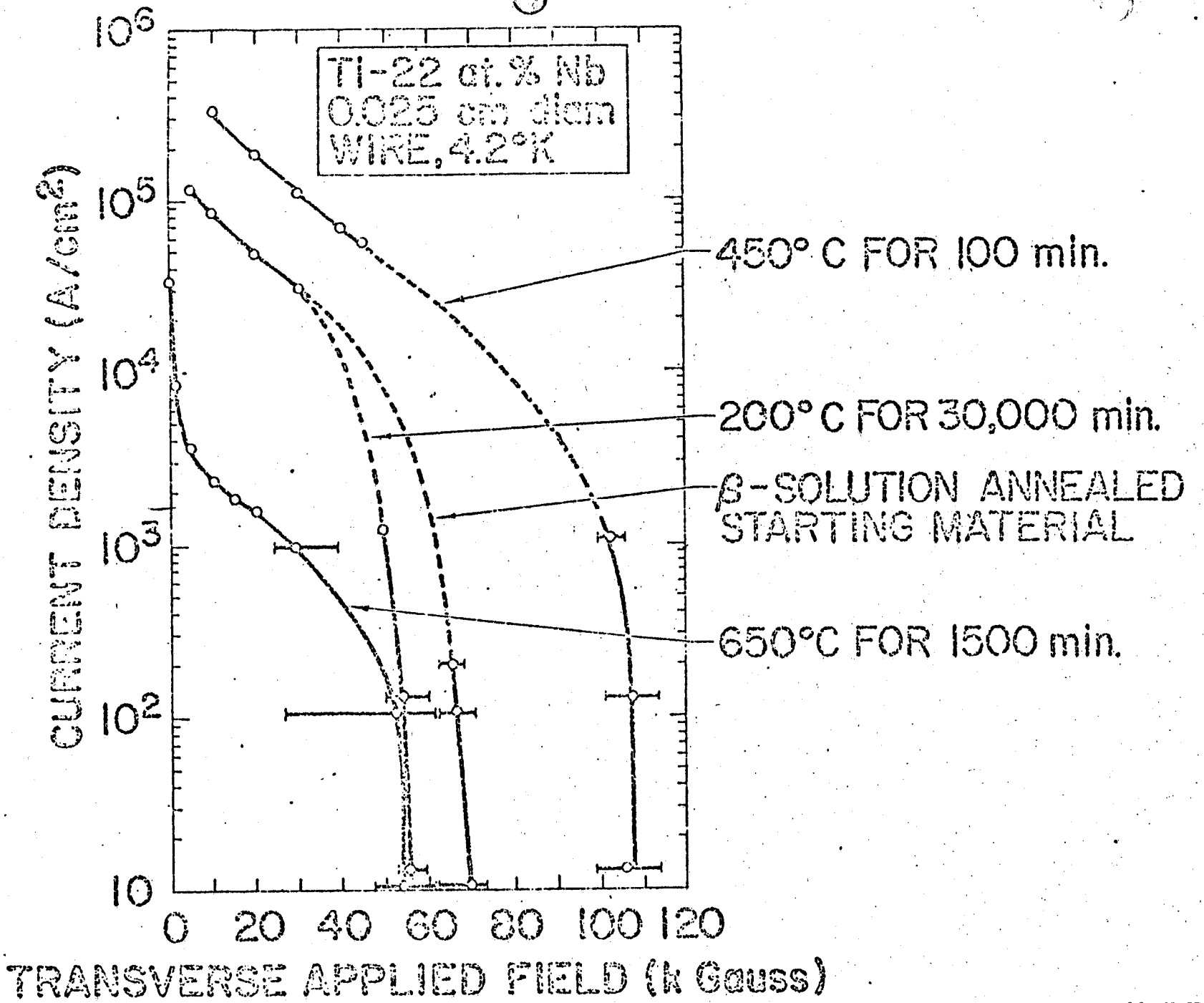

4-20-65

00-153157

FIGURE 11

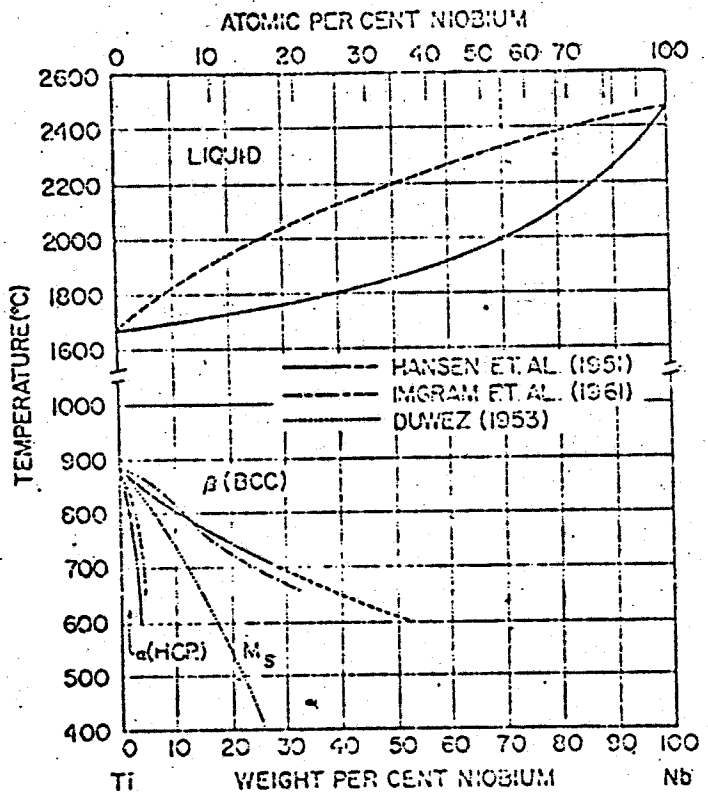

—The Ti-Nb alloy diagram.

FIGURE 12

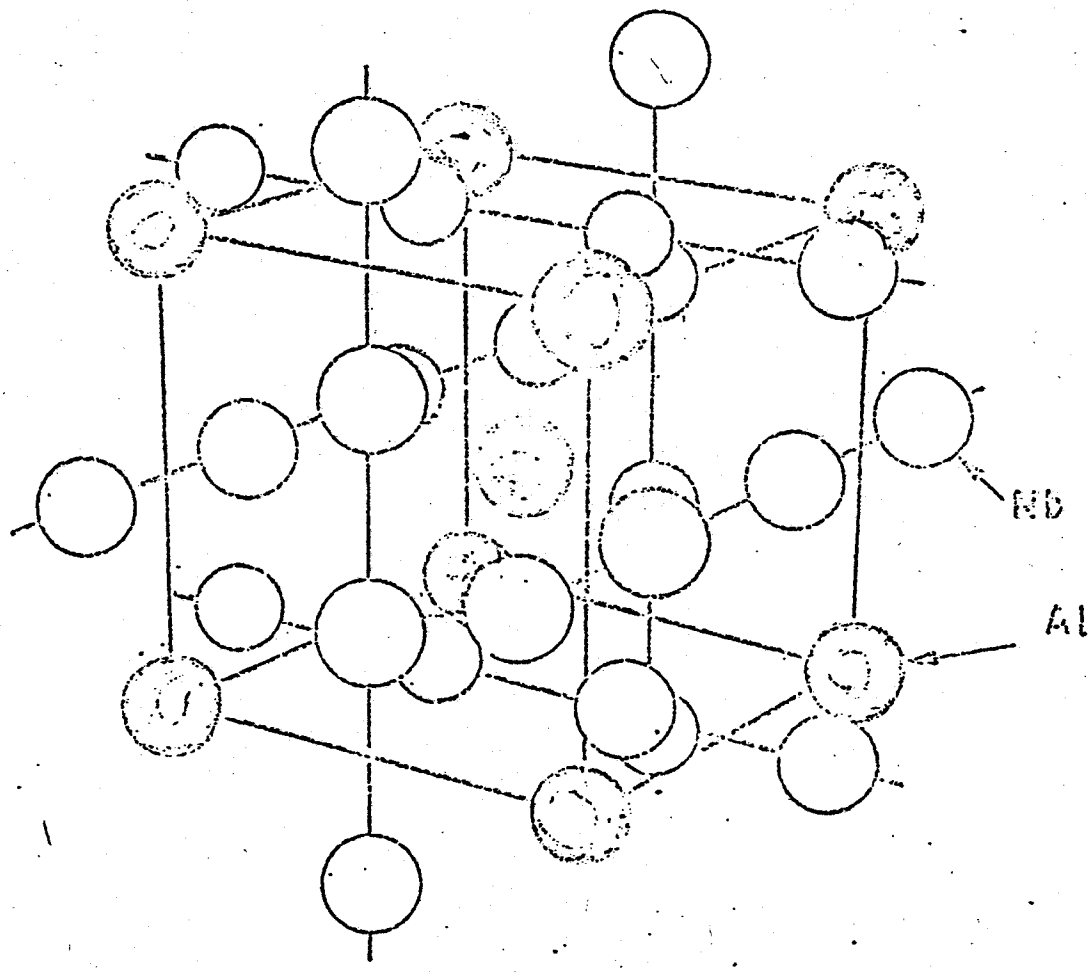

Figure 13 Unit Cell of the β-Tungsten Crystal Structure of Nb_3Al.

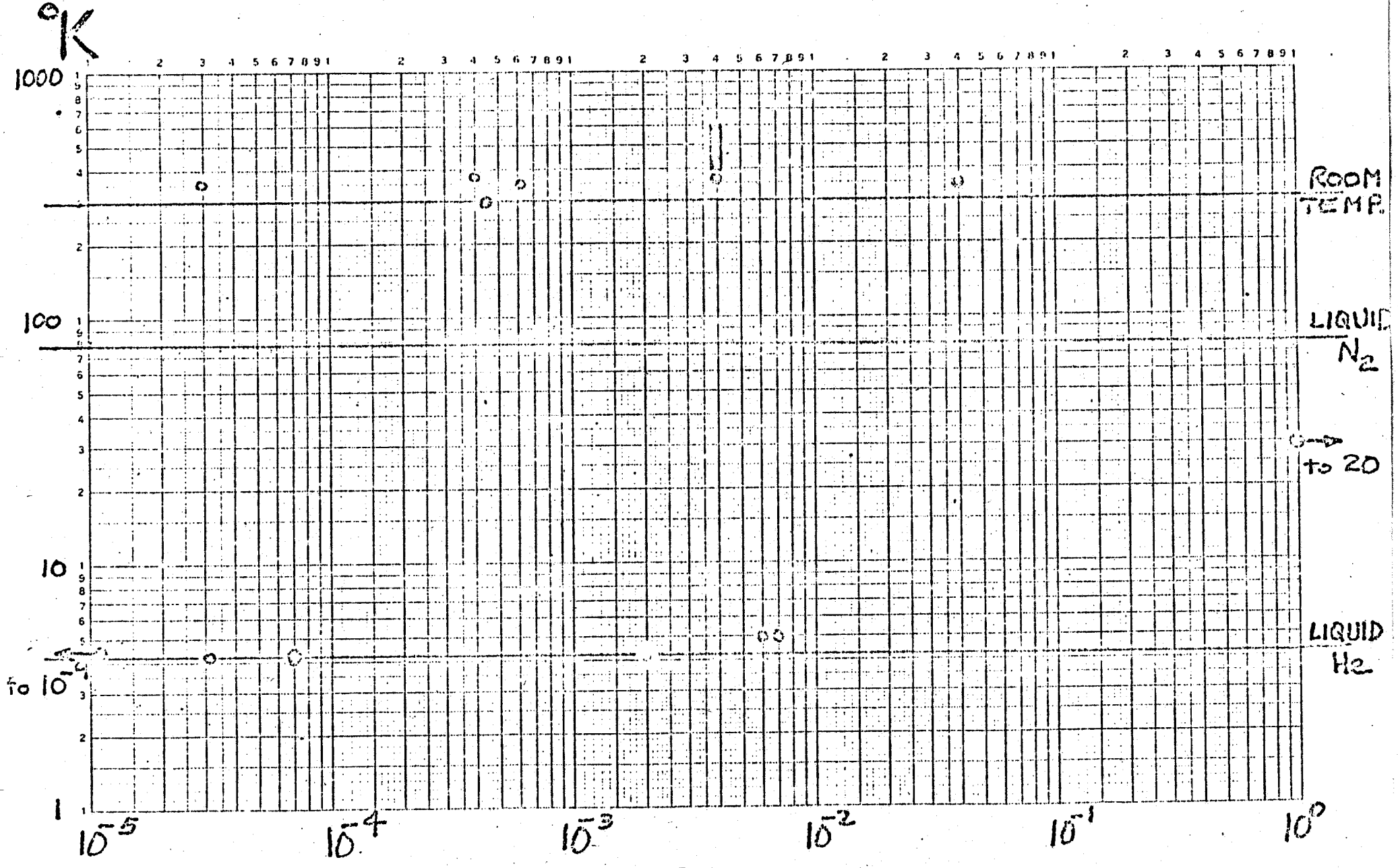

FIGURE 14 DISPLACEMENTS PER ATOM

FIGURE 15

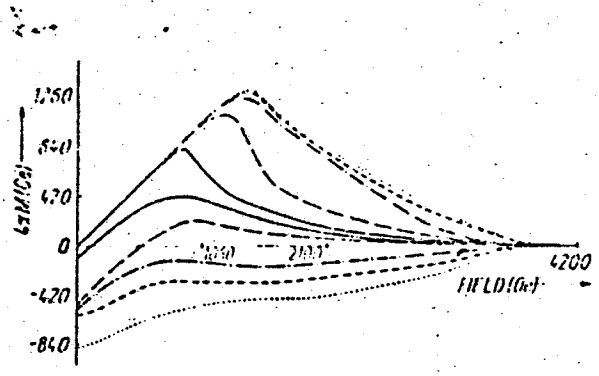

A Magnetization curves for cold rolled niobium specimens
degassed specimen, 14% deformed, 35% deformed,
62.5% deformed, 62.5% deformed and repeatedly bent

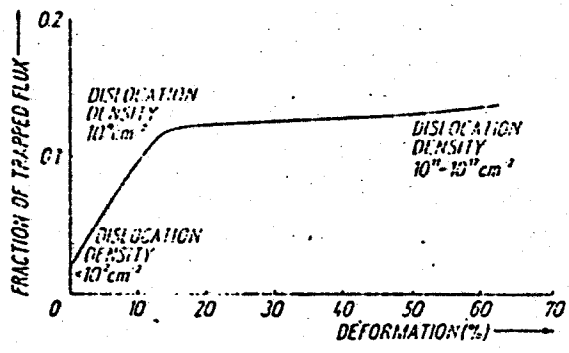

B

FIGURE 16

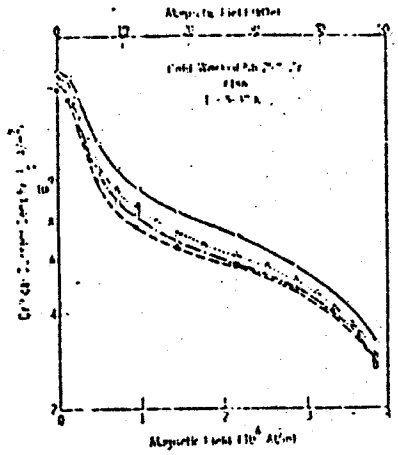

A. Critical current density versus applied transverse magnetic field [Expressed in Ampere turns per meter]. Open circles, pre-irradiation; closed circles, 1.1×10^{21} (15-MeV) d/m^2; squares, post 77°K; triangles, post 300°K.

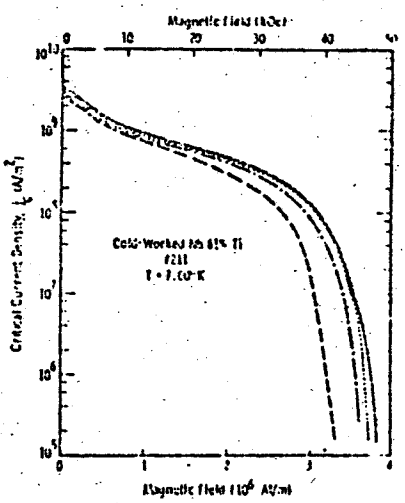

B. Critical current density versus applied transverse magnetic field. Solid line, pre-irradiation; dashed line, 1.0×10^{21} (15-MeV) d/m^2; dash-dot line, post 77 °K; dotted line, post 300° K.

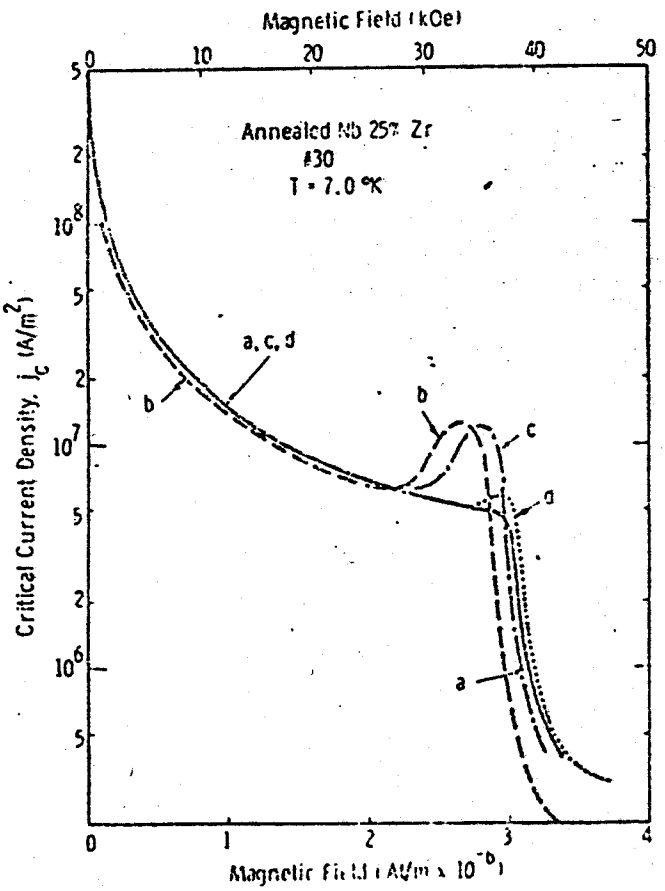

C. Critical current density vs applied transverse magnetic field. (*a*) , preirradiation; (*b*)----------, 10^{21} 15-MeV deuterons/cm^2; (*c*)— — —, post-77 K anneal; (*d*)·····, post-300 K anneal.

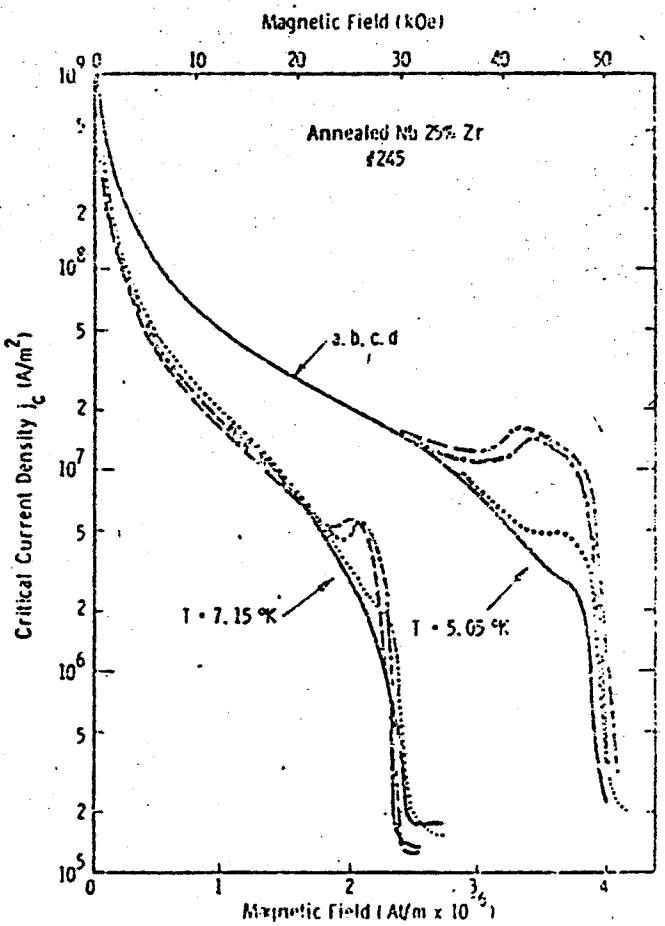

D. Critical current density vs applied transverse magnetic field. (*a*) , preirradiation; (*b*)----------, 10^{21} 15-MeV deuterons/cm^2; (*c*)— — —, post-77 K anneal; (*d*) ·····, post-300 K anneal.

FIGURE 18

Stability

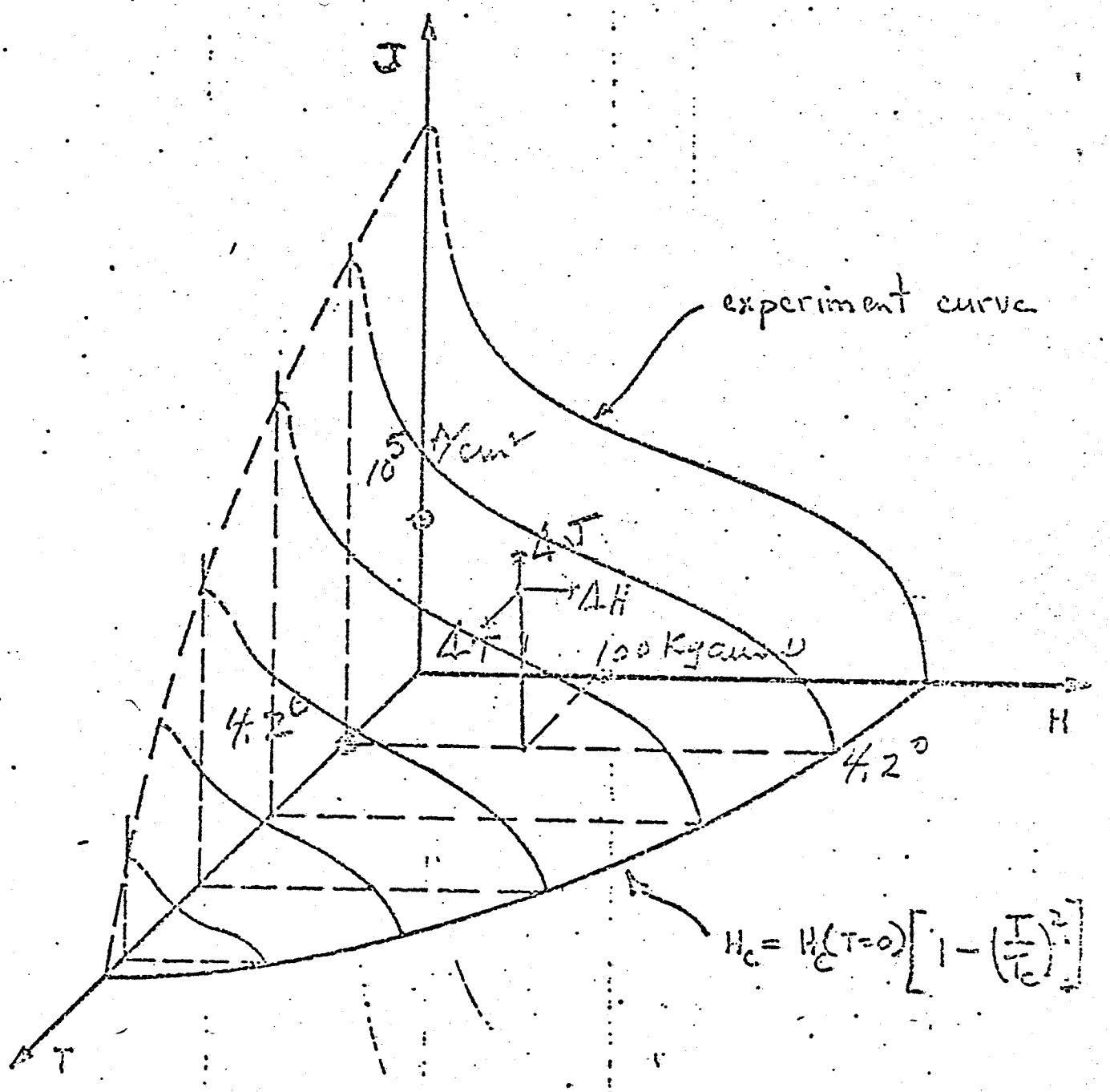

ΔJ, ΔH, or ΔT can drive a superconductor normal

FIGURE 19

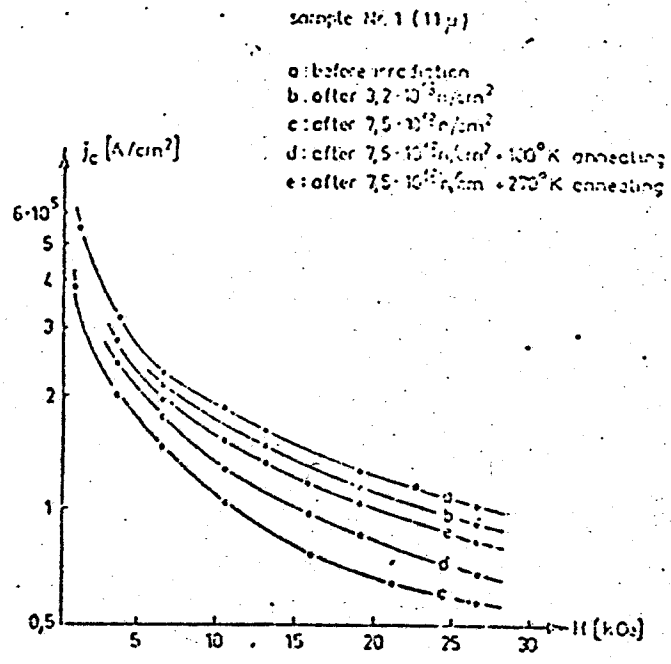

A : Critical current of an NbTi wire (11 μ) versus a transverse magnetic field at 5.3°K before and after neutron irradiation. (The zero field value of curve a is 1.2×10^6 A/cm²)

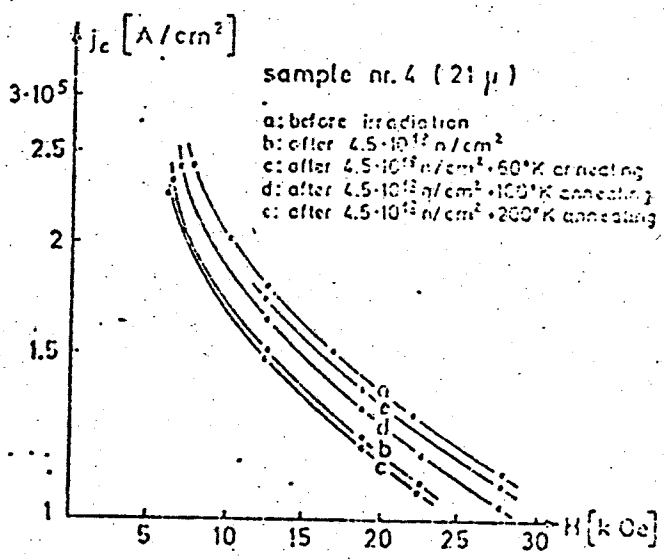

B : Critical current of an NbTi wire (21 μ) versus a transverse magnetic field at 5.3°K before and after neutron irradiation.

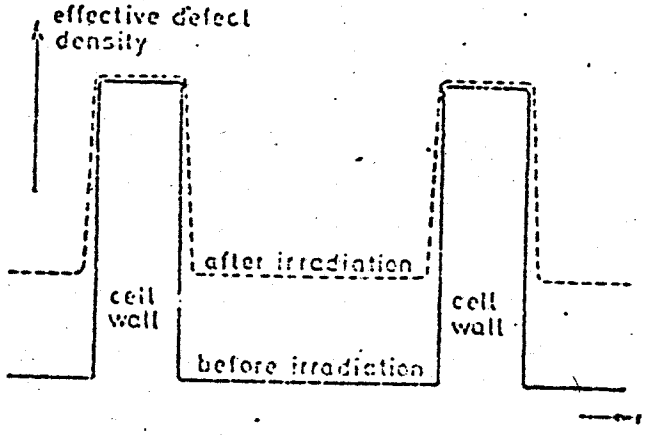

C : Effective defect density for flux pinning across a cell.

FIGURE 20

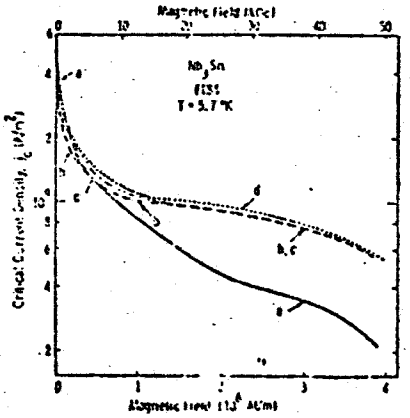

A . Critical current density versus applied transverse magnetic field. See caption of Fig. 6 for meaning of symbols.

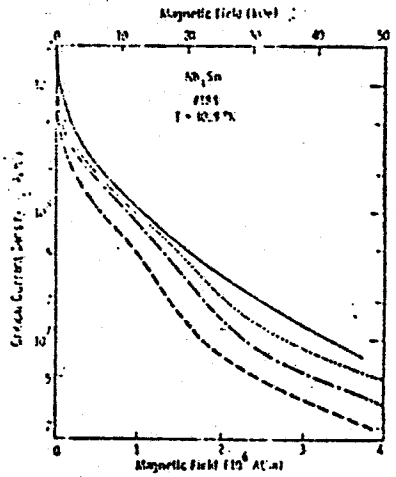

B . Critical current density versus applied transverse magnetic field. See caption of Fig. 6 for meaning of symbols.

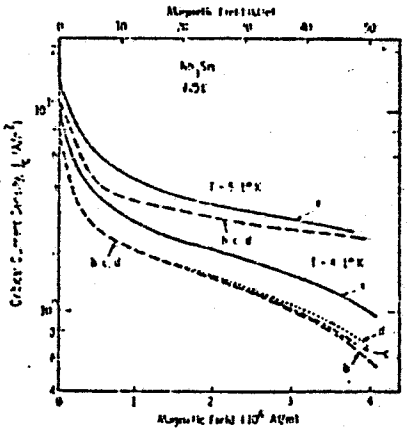

C . Critical current density versus applied transverse magnetic field. See caption of Fig. 6 for meaning of symbols.

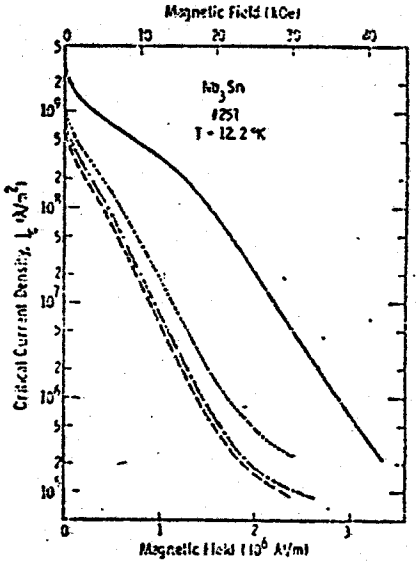

D . Critical current density versus applied transverse magnetic field. See caption of Fig. 6 for meaning of symbols.

FIGURE 21

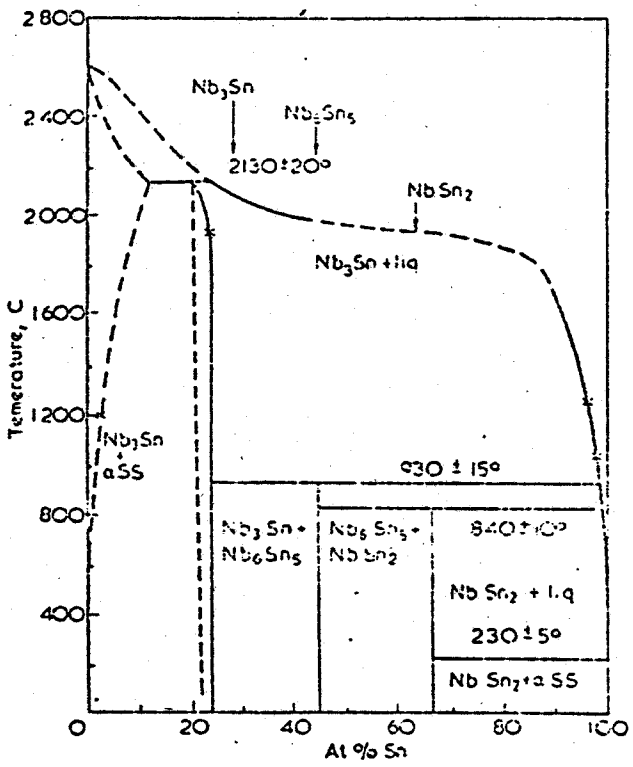

. Probable phase diagram for NbSn system according to references 42, 45, and 46

FIGURE 22

Initial sample characteristics and current carrying behavior as a function of irradiation.

J_c rating	Sample	Composition (wt %, Sn)	T_c midpoint (°K)	ΔT_c (°K)	ϕ (neutrons/cm²) $\times 10^{-17}$	J_{c1} (kG-A/cm²) $\times 10^{-6}$ // 10 kG	J_{c1} (kG-A/cm²) $\times 10^{-6}$ // 11 kG	(kG-A/cm²) $\times 10^{-6}$ α_1	α_2
low	FS 20(5)	29.5 ± 0.5*	18.3*	0.01	0	1.36	1.33	1.49	...
					3.4	5.30	6.46	6.58	14.3
					7.2	9.38	11.1	11.3	28.6
					10.5	13.0	16.8	24.1	90.5
					14.0	15.0	18.2	35.0	76.0
medium	78(3)	28.0 ± 0.1	16.1	0.80	0	4.0	4.48	6.5	...
					3.3	6.6	7.81	12.1	...
					6.9	8.0	9.66	15.6	...
					10.1	6.2	7.56	10.1	19.5
high	71(1)	29.2 ± 0.1	16.9	0.80	0	11.5	13.3	19.4	27.9
					3.4	11.7	14.1	19.2	29.7
					7.2	0.89	1.3	1.18	2.32

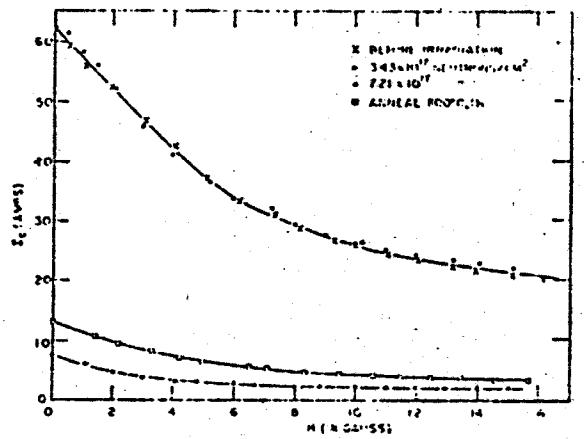

Current-carrying characteristics before and after irradiation vs perpendicular applied field [sample 74(4)].

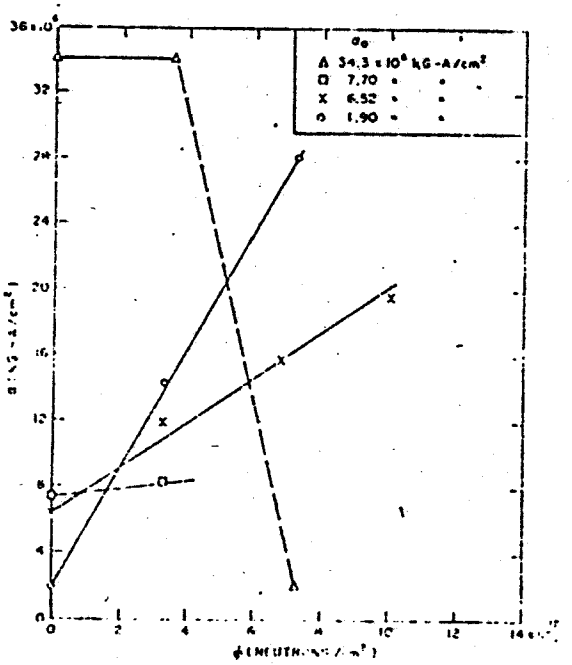

Value of α as a function of neutron dose for samples with various initial values of α_1.

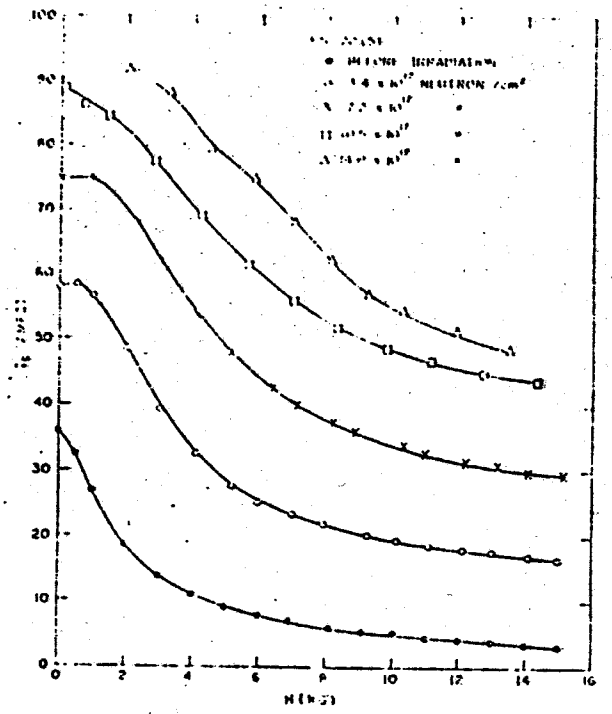

Current-carrying characteristics before and after irradiation vs perpendicular applied field [sample FS 20(5)].

FIGURE 23

98/4

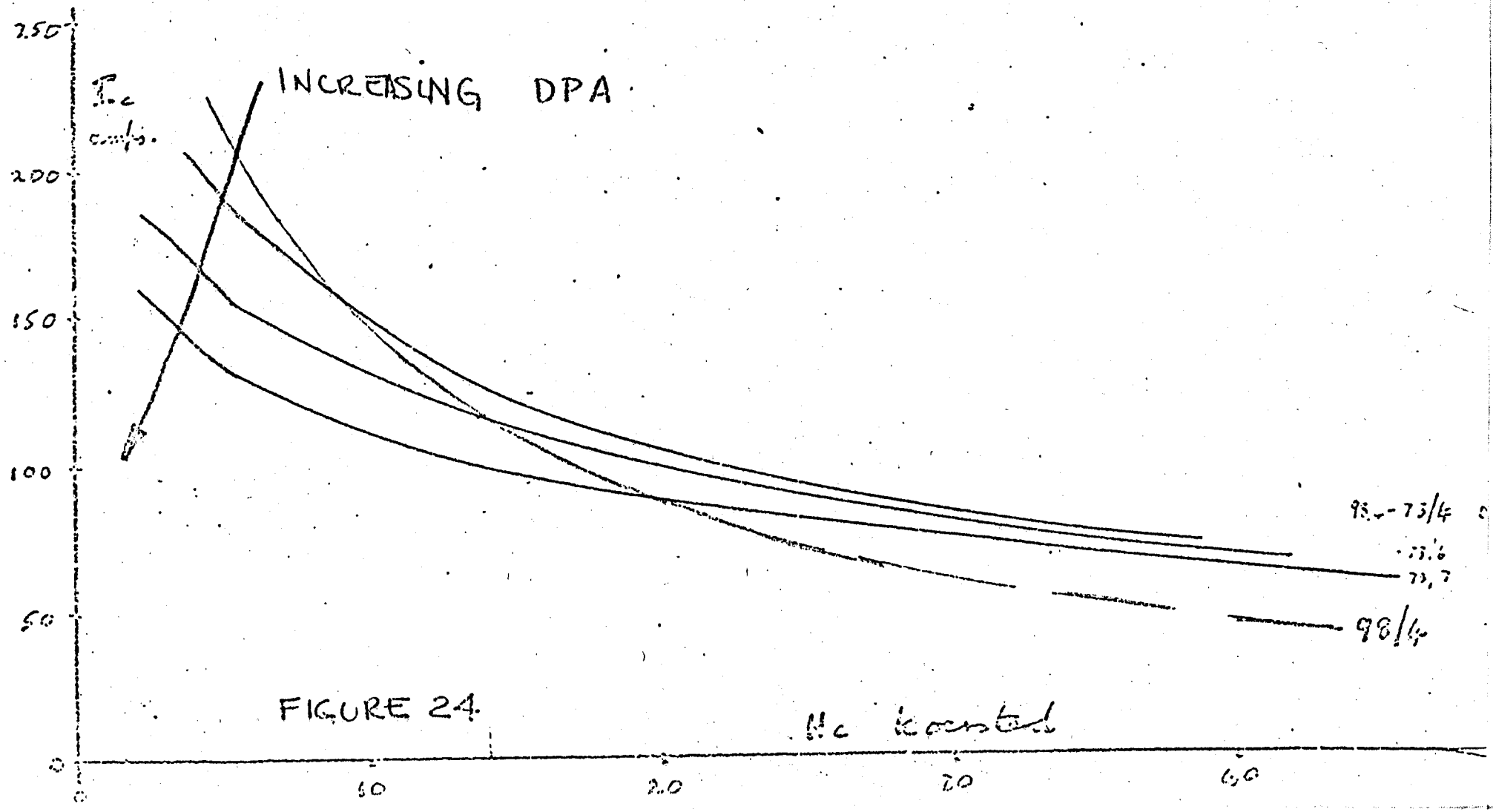

FIGURE 24

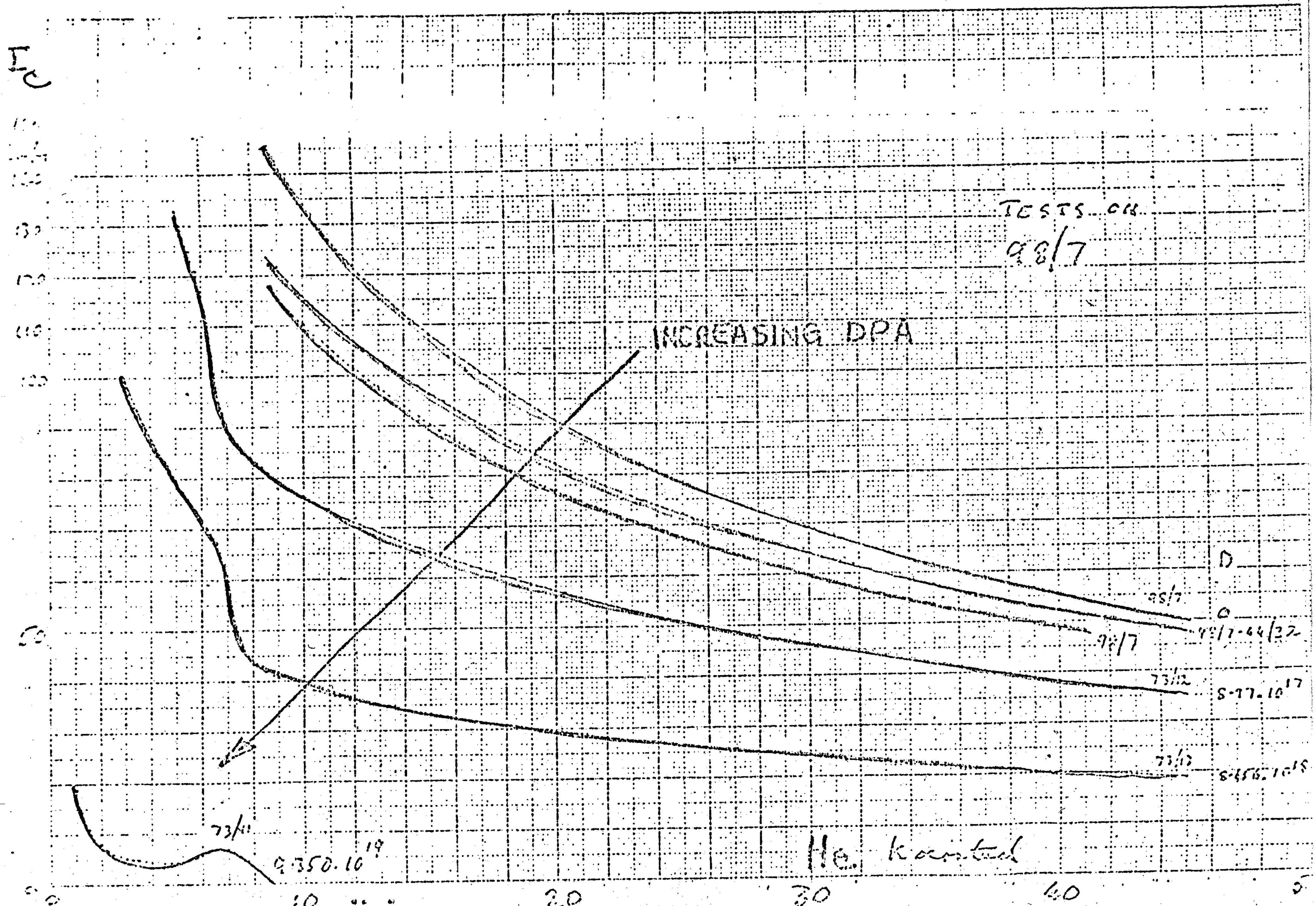

I_c
Tests on 98/7
INCREASING DPA
D
98/7
0
98/7-44/32
73/12
5-77.10^17
73/13
73/11
9350.10^19
He. Koristed
10
20
30
40

FIGURE 25

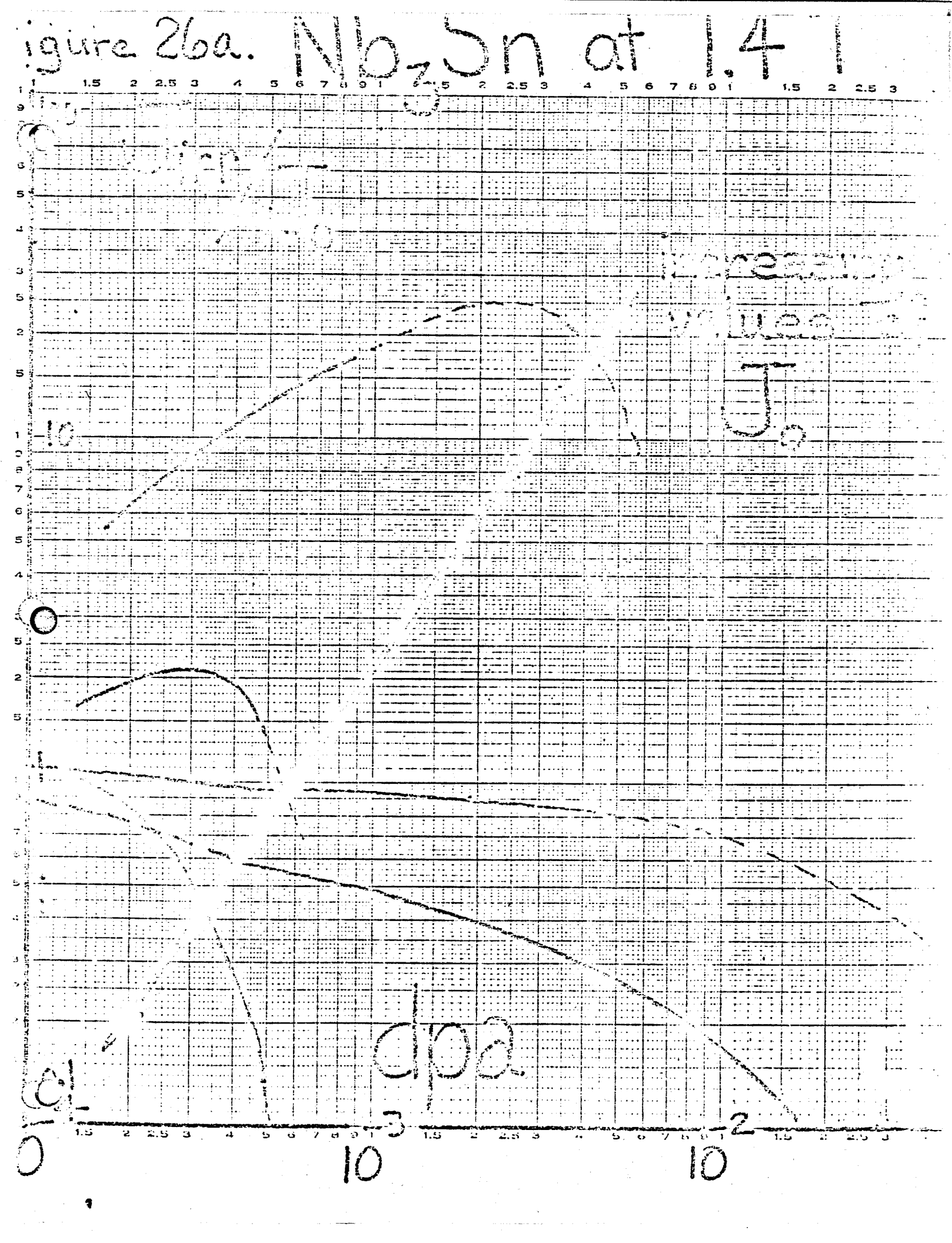
Figure 26a. Nb3Sn at 1.4 K
1.5 2 2.5 3 4 5 6 7 8 9 1 1.5 2 2.5 3 4 5 6 7 8 9 1 1.5 2 2.5 3
10
0
10
10

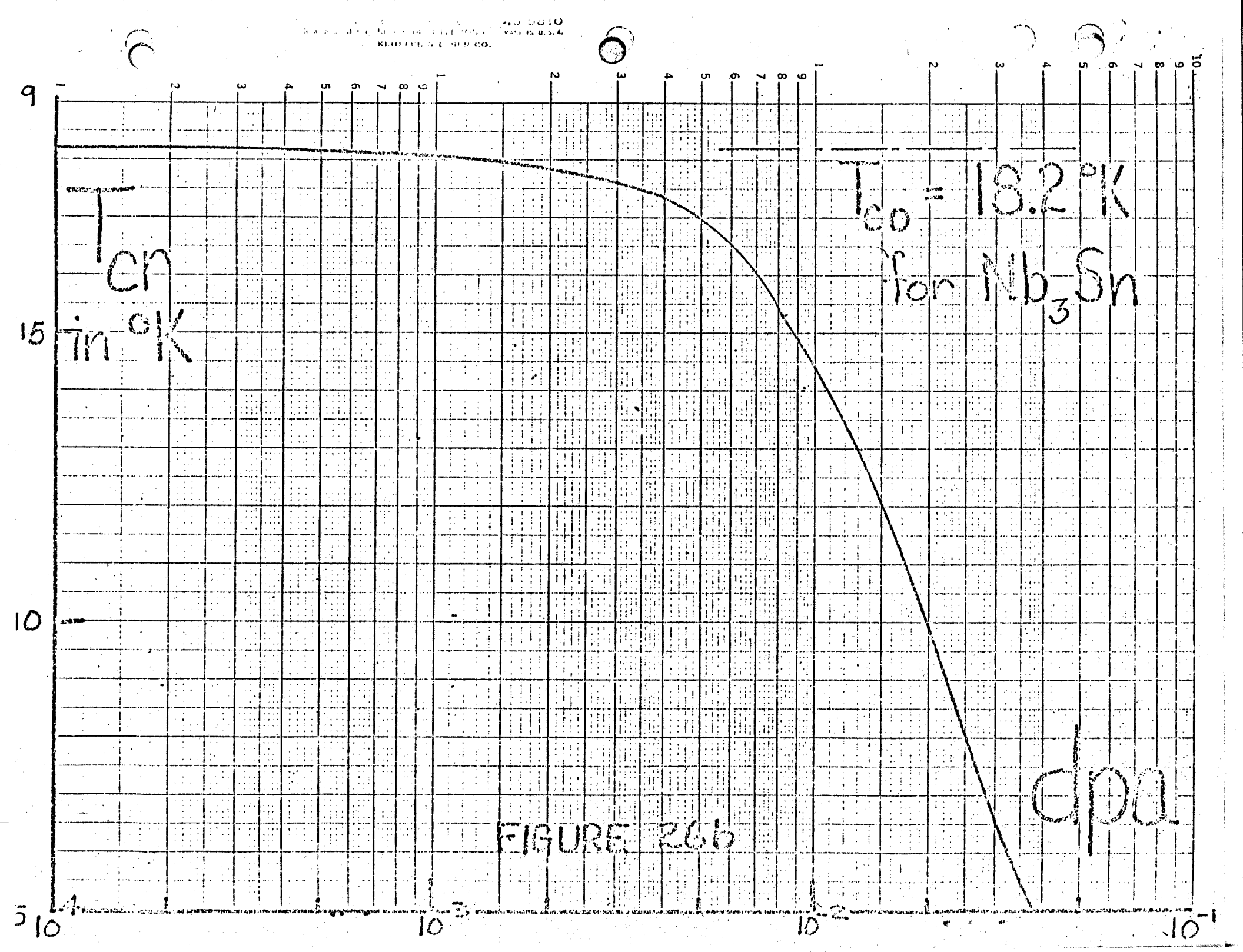

FIGURE 26b

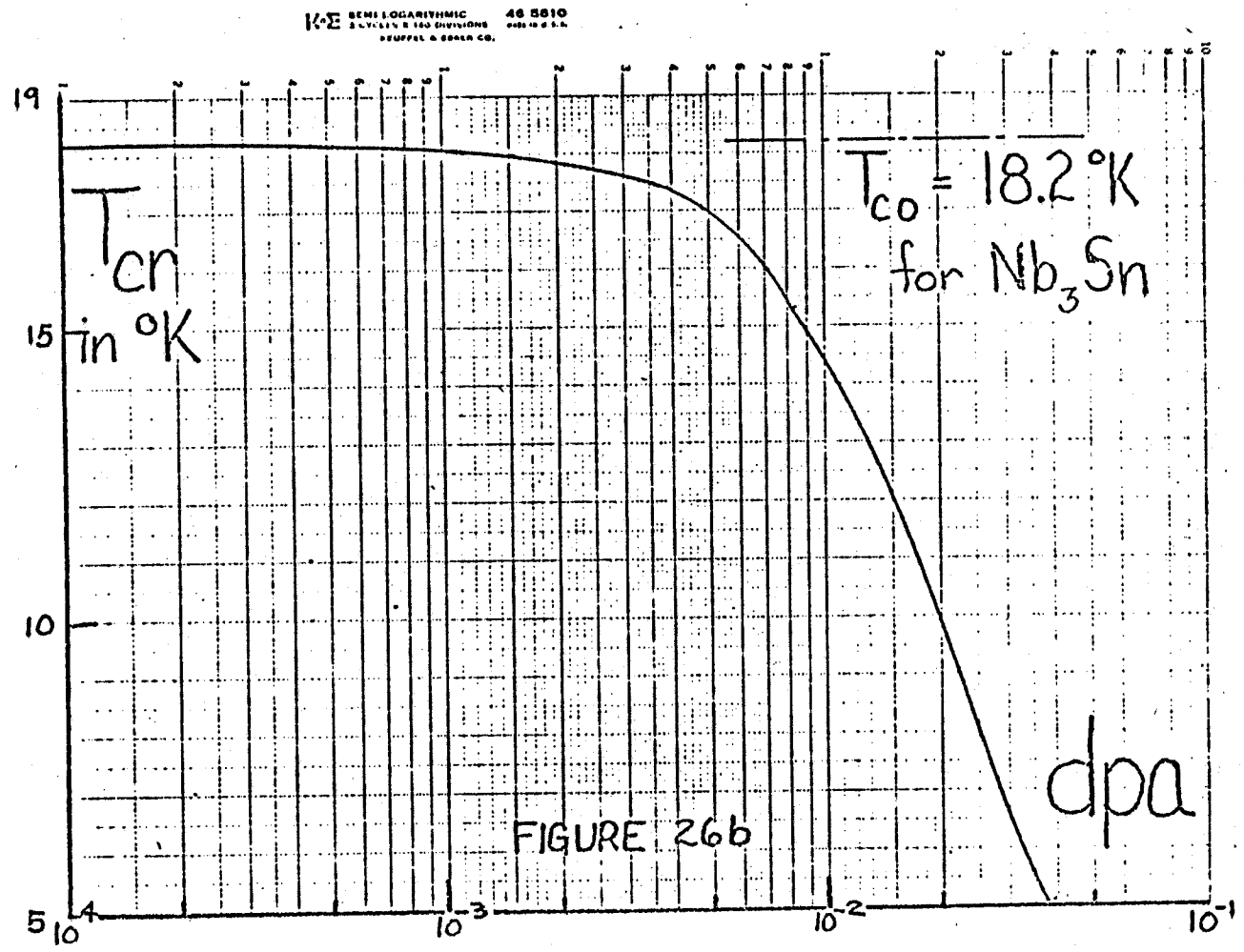
K-E SEMI-LOGARITHMIC 46 5810
T_{cn} in °K
T_{co} = 18.2 °K for Nb_3Sn
dpa
19
15
10
5
10^{-4}
10^{-3}
10^{-2}
10^{-1}

FIGURE 26b

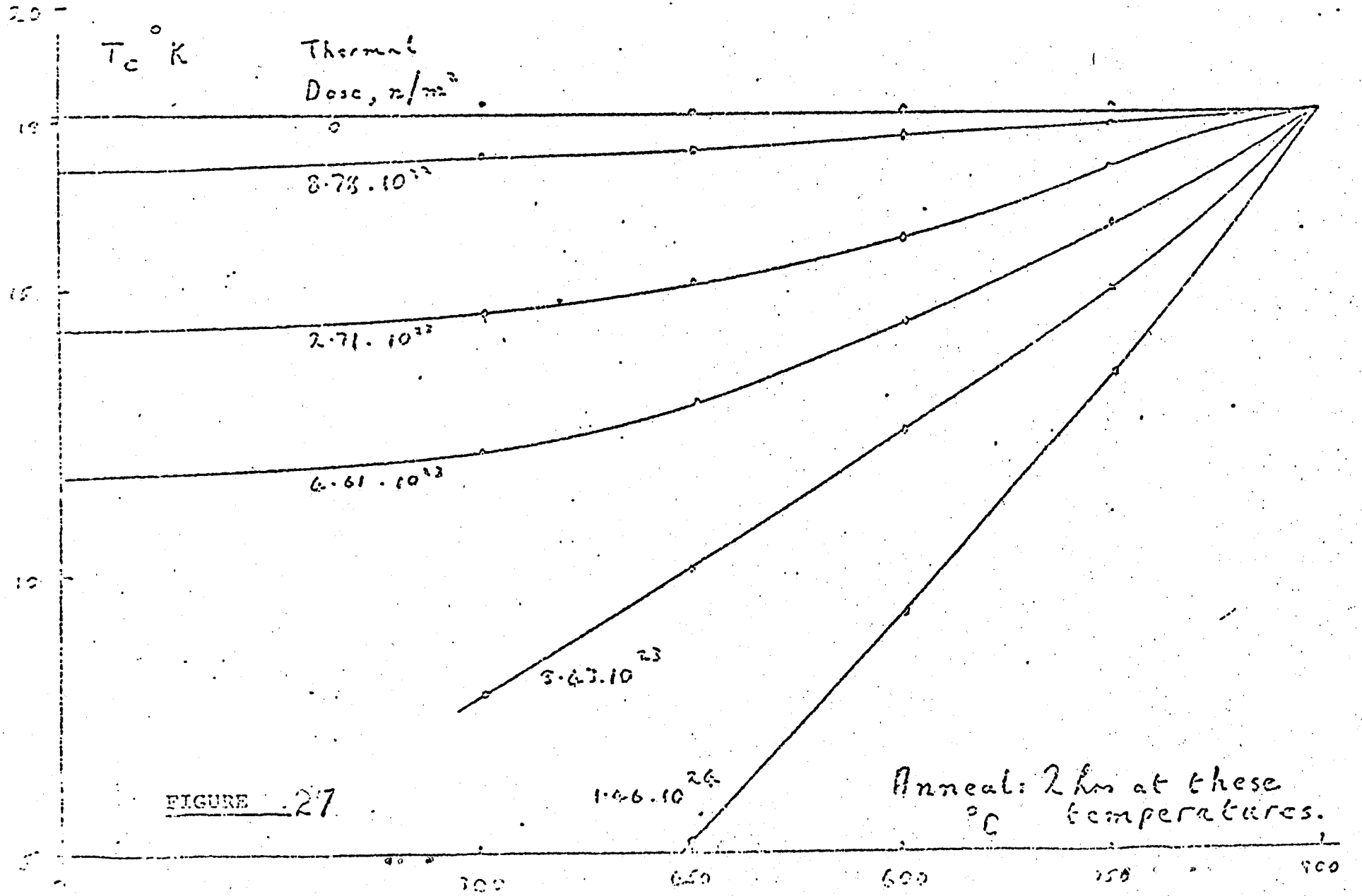
T_c °K
Thermal Dose, n/m²
0
8·78 . 10²²
2·71 . 10²³
6·61 . 10²³
3·43 . 10²³
1·06 . 10²⁴
Anneal: 2 hr at these °C temperatures.
20
15
10
5
300
600
900

FIGURE 27

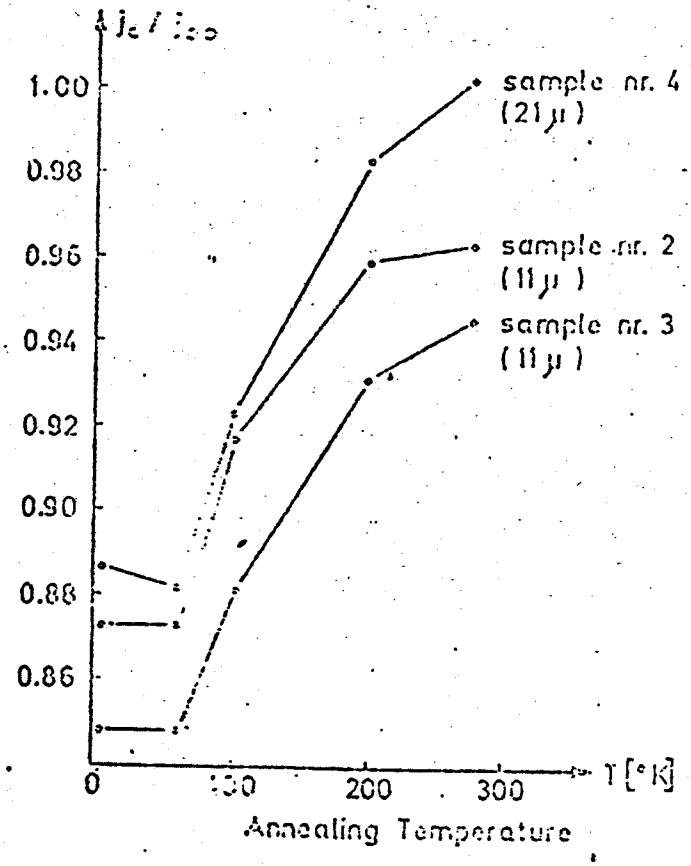

: Recovery of the critical current (normalized to the value before irradiation) of the samples 2, 3, 4.

FIGURE 28

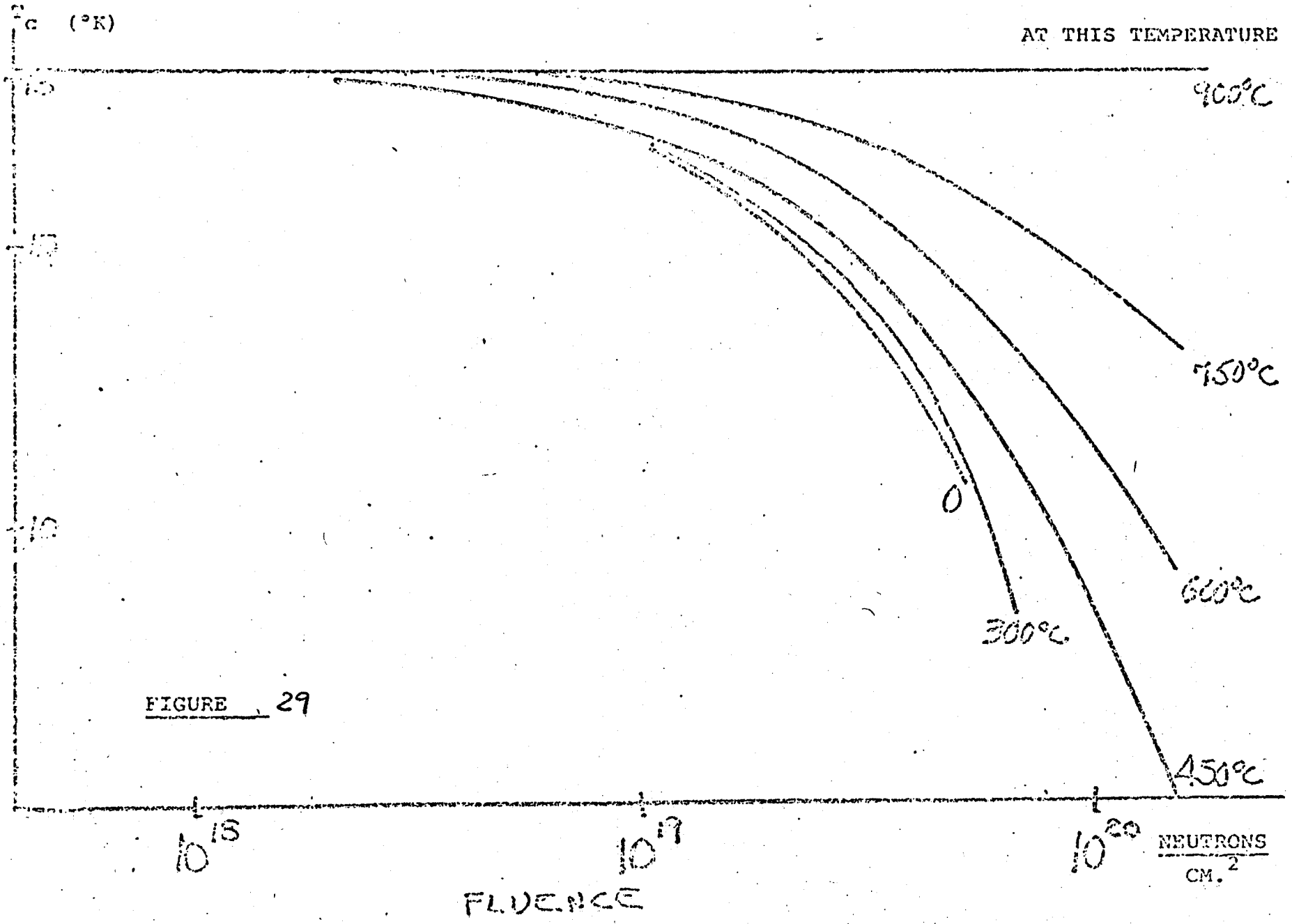
ANNEAL TWO HOURS
AT THIS TEMPERATURE
T_c (°K)
15
10
5
900°C
750°C
600°C
300°C
0
450°C
10^{18}
10^{19}
10^{20}
NEUTRONS / CM.^{2}
FLUENCE

FIGURE 29

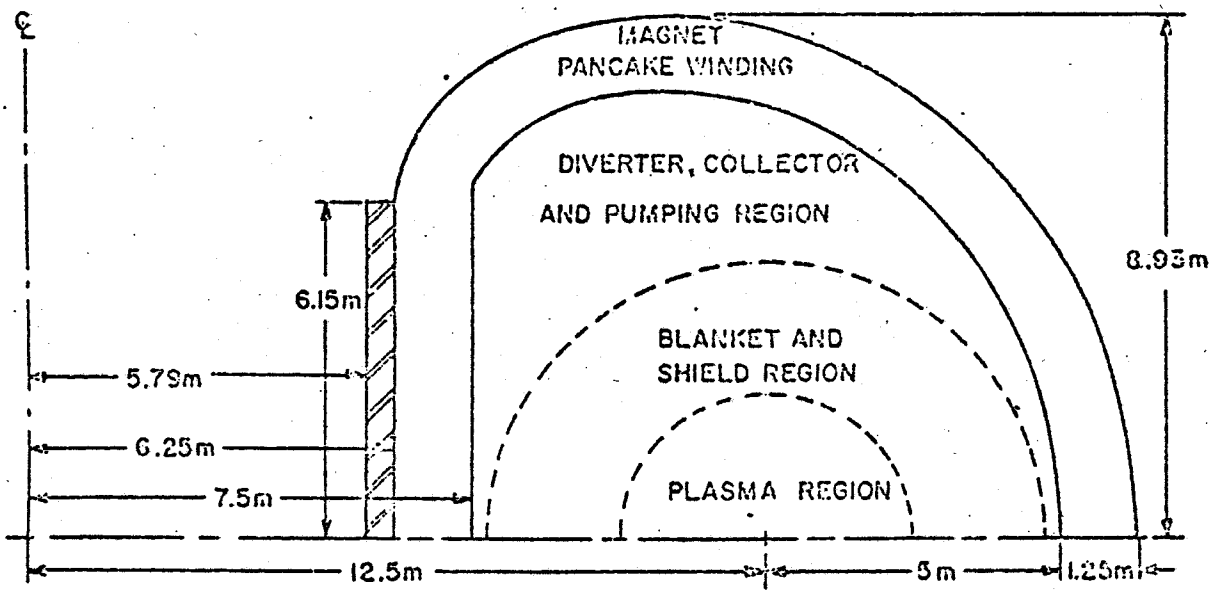

FIGURE 30a

Toroidal magnet cross section.

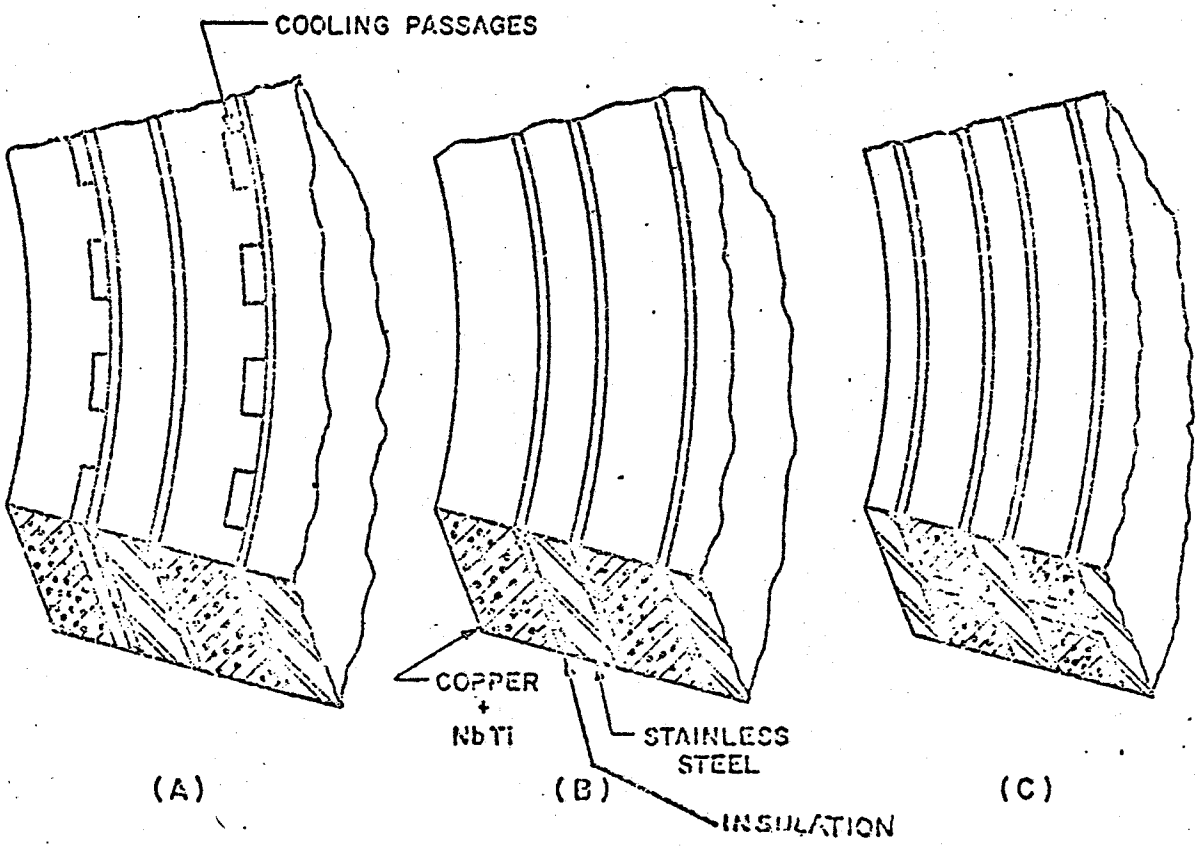

Pancake designs.

FIGURE 30b

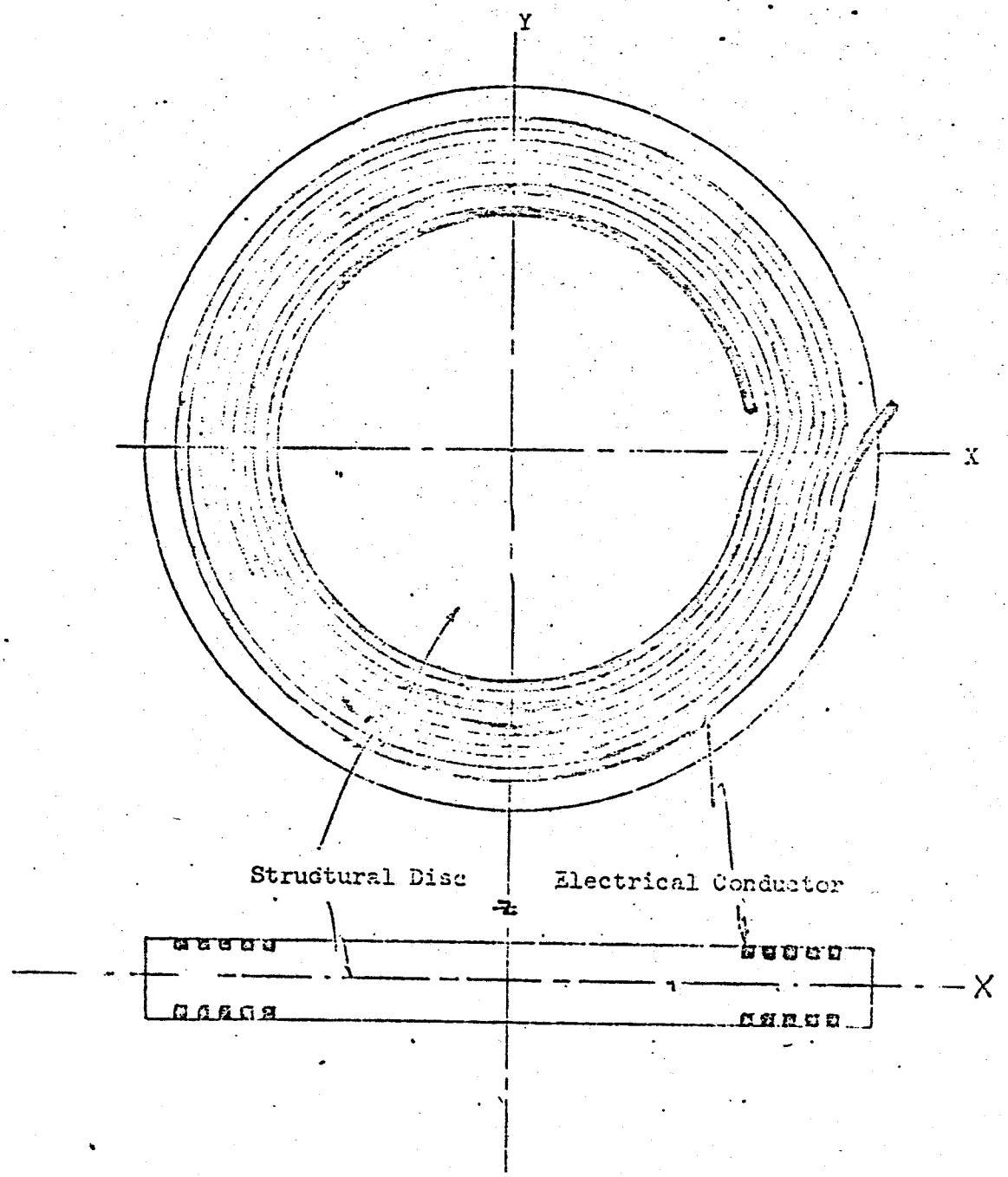

Figure 3

Figure 32 a

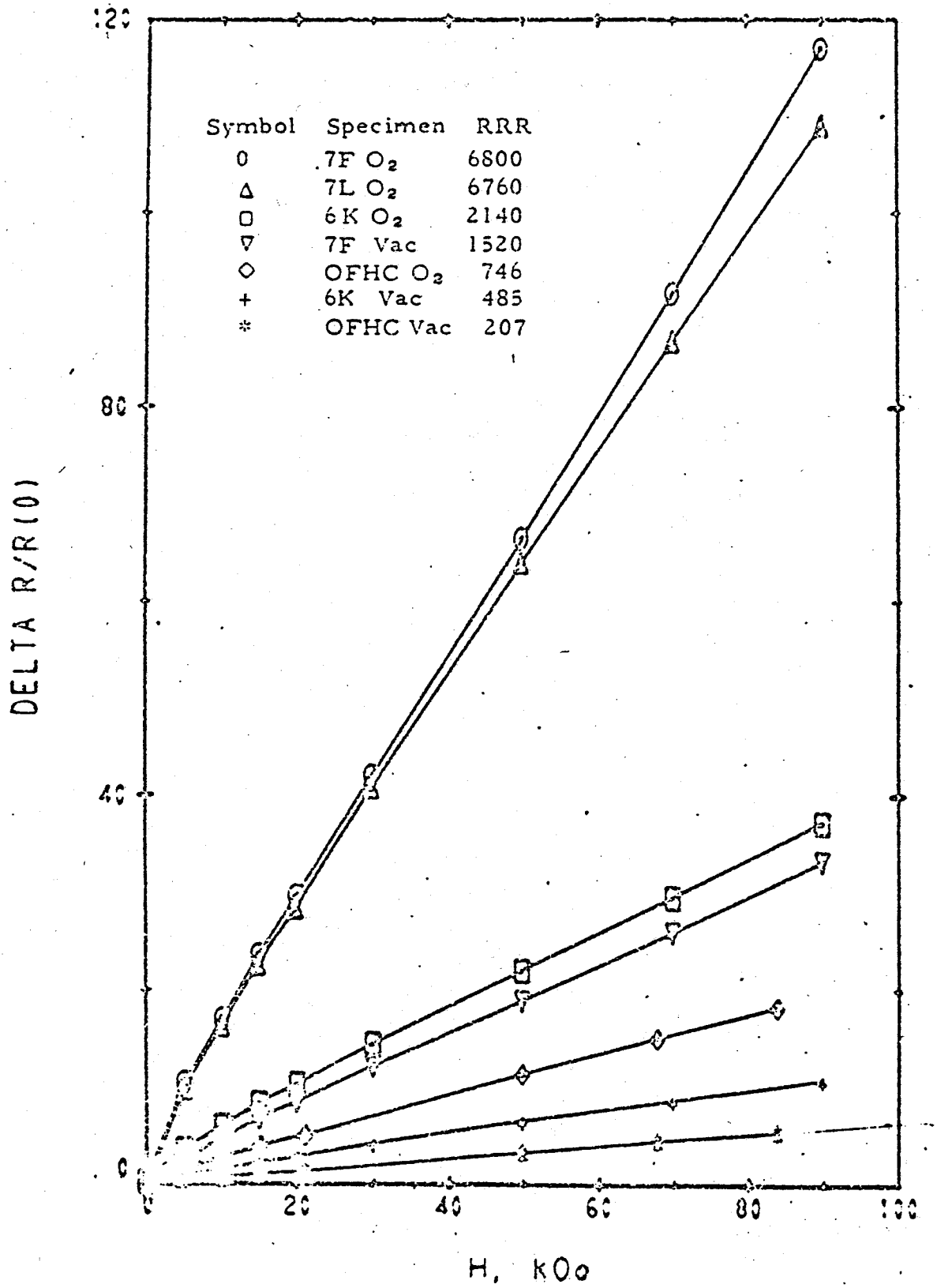

15/27/72 MAGNETORESISTANCE VS. PURITY AT T=4K

Figure 32 b

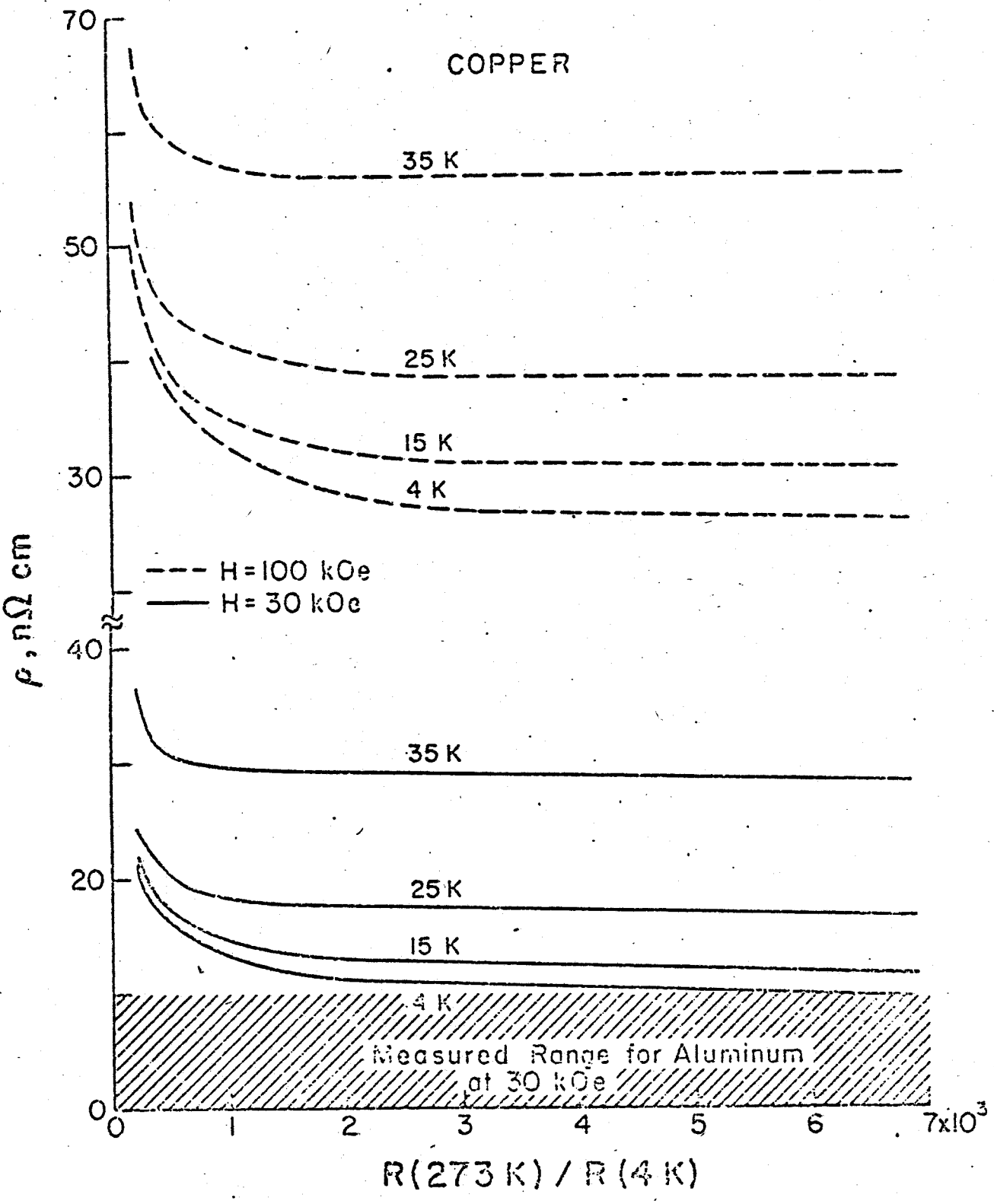
COPPER
35 K
25 K
15 K
4 K
H = 100 kOe
H = 30 kOe
35 K
25 K
15 K
4 K
Measured Range for Aluminum at 30 kOe
ρ, nΩ cm
70
50
30
40
20
0
0
1
2
3
4
5
6
7x10³
R(273 K) / R(4 K)

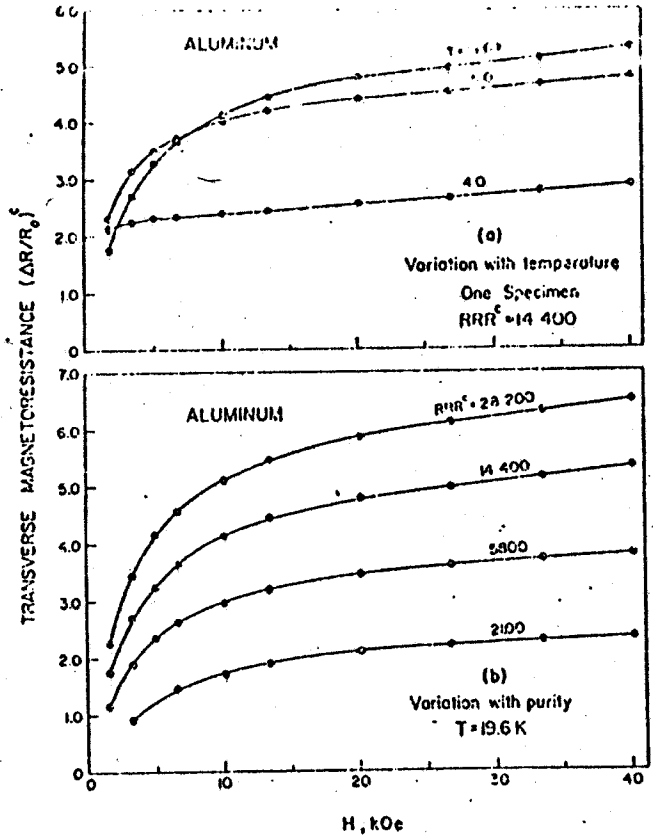

Fig. 33a Transverse magnetoresistance data for polycrystalline aluminum wires. The superscript c indicates that the zero field data have been corrected for size effect.

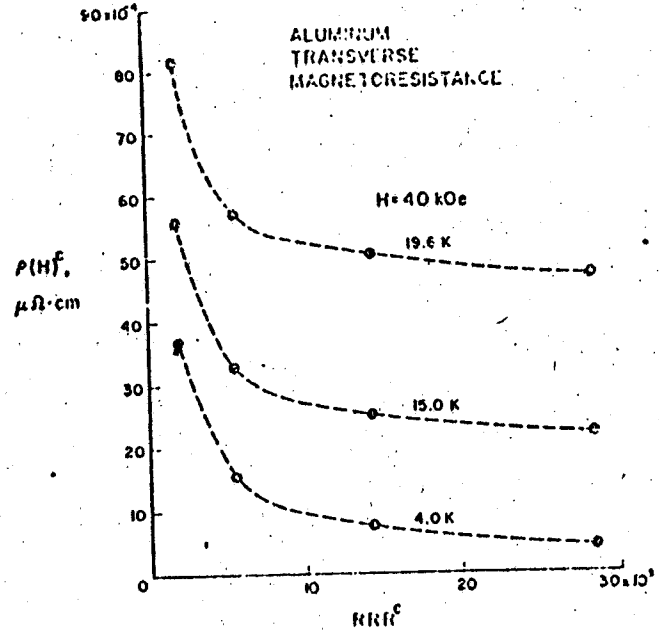

Fig. 33b Resistivity of aluminum specimens at 40 kOe. The superscript c indicates that the zero field data have been corrected for size effect.

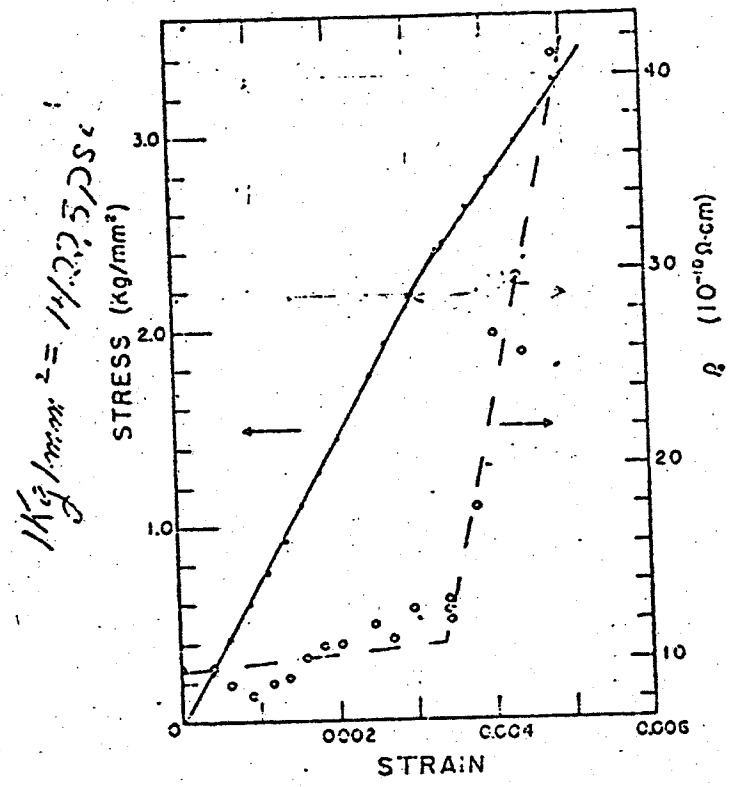

FIG. 33c The stress-strain curve and the residual resistivity versus strain at 4.4° K for a specimen with the (211) direction parallel to the axis (circles of Fig. 1).

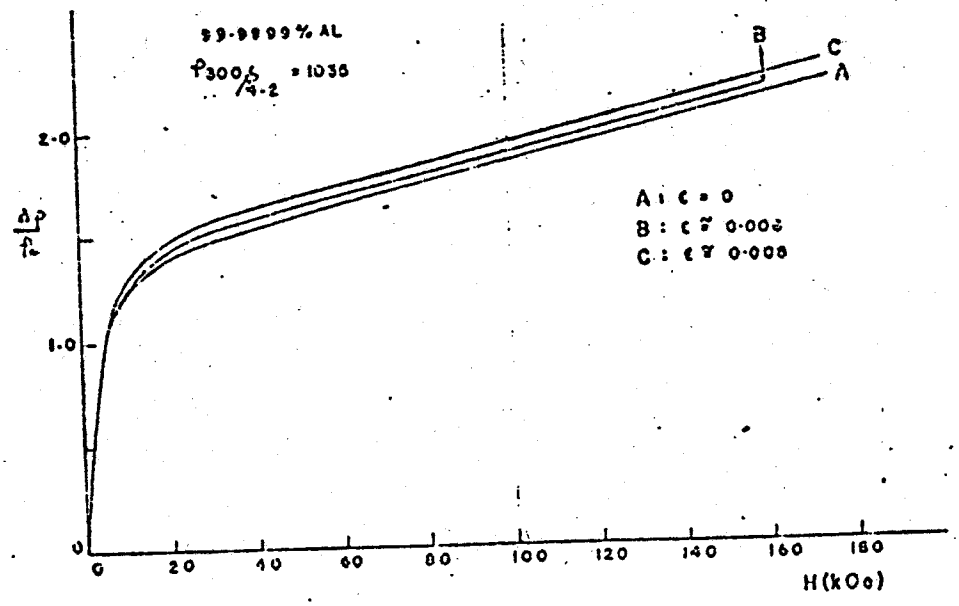

FIG. 33d Magnetoresistance at 4.2 °K of the 69 purity aluminium showing strain effects on different samples.

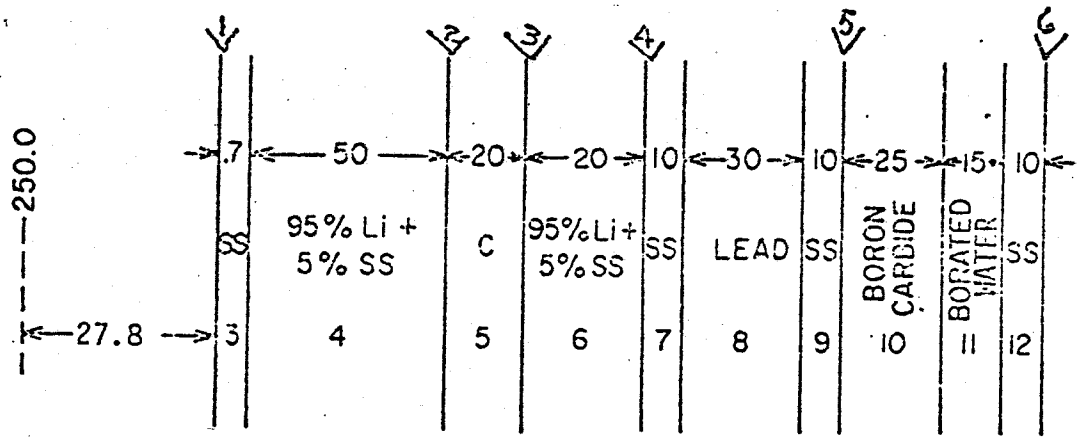

SCHEMATIC OF BLANKET AND SHIELD

FIGURE 34

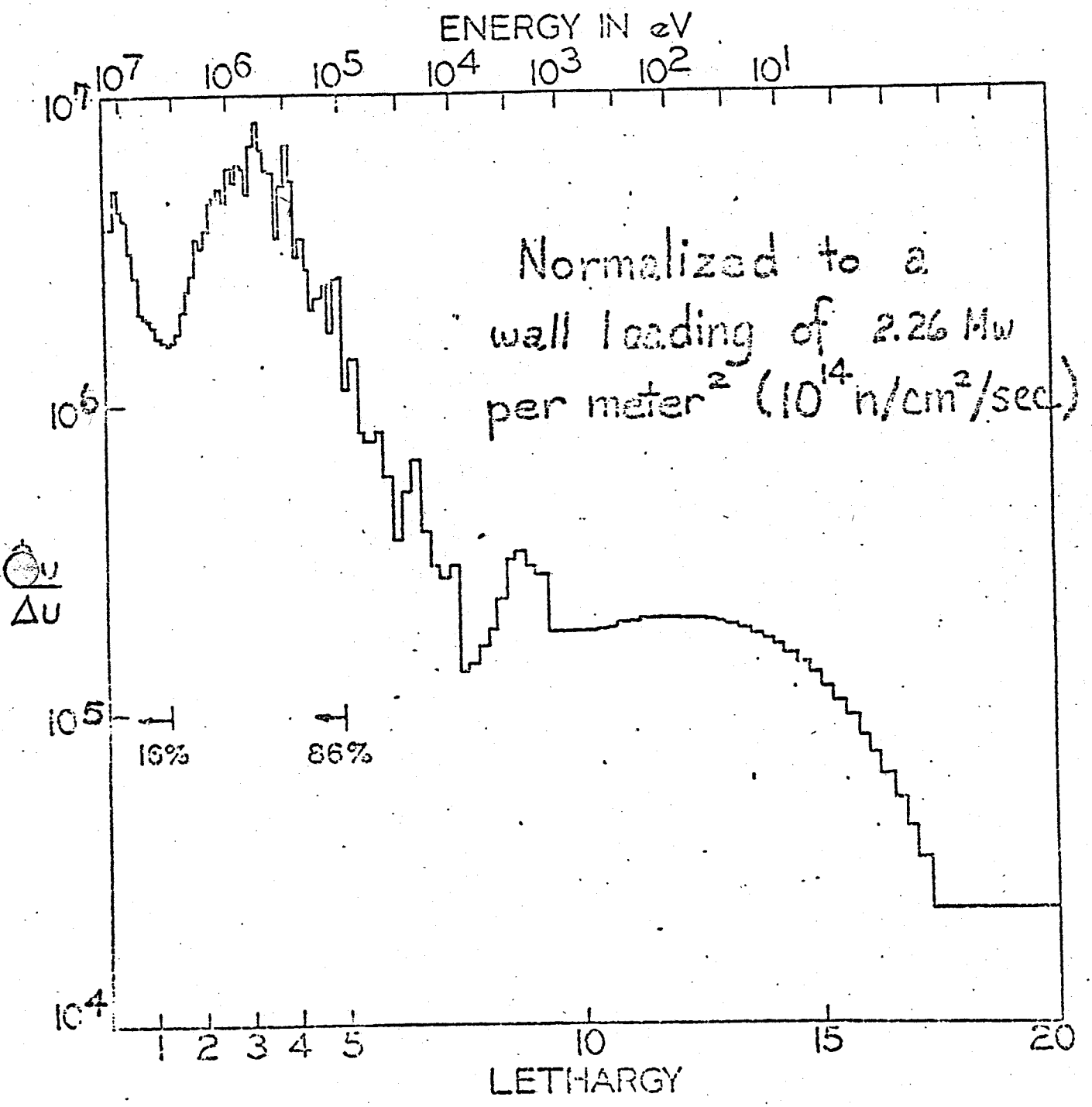
ENERGY IN eV
10^7 10^6 10^5 10^4 10^3 10^2 10^1
Normalized to a wall loading of 2.26 Mw per meter^2 (10^{14} n/cm^2/sec)
$\frac{\Delta u}{\Delta u}$
10^6
10^5
10^4
16%
86%
1 2 3 4 5 10 15 20
LETHARGY

FIGURE 35

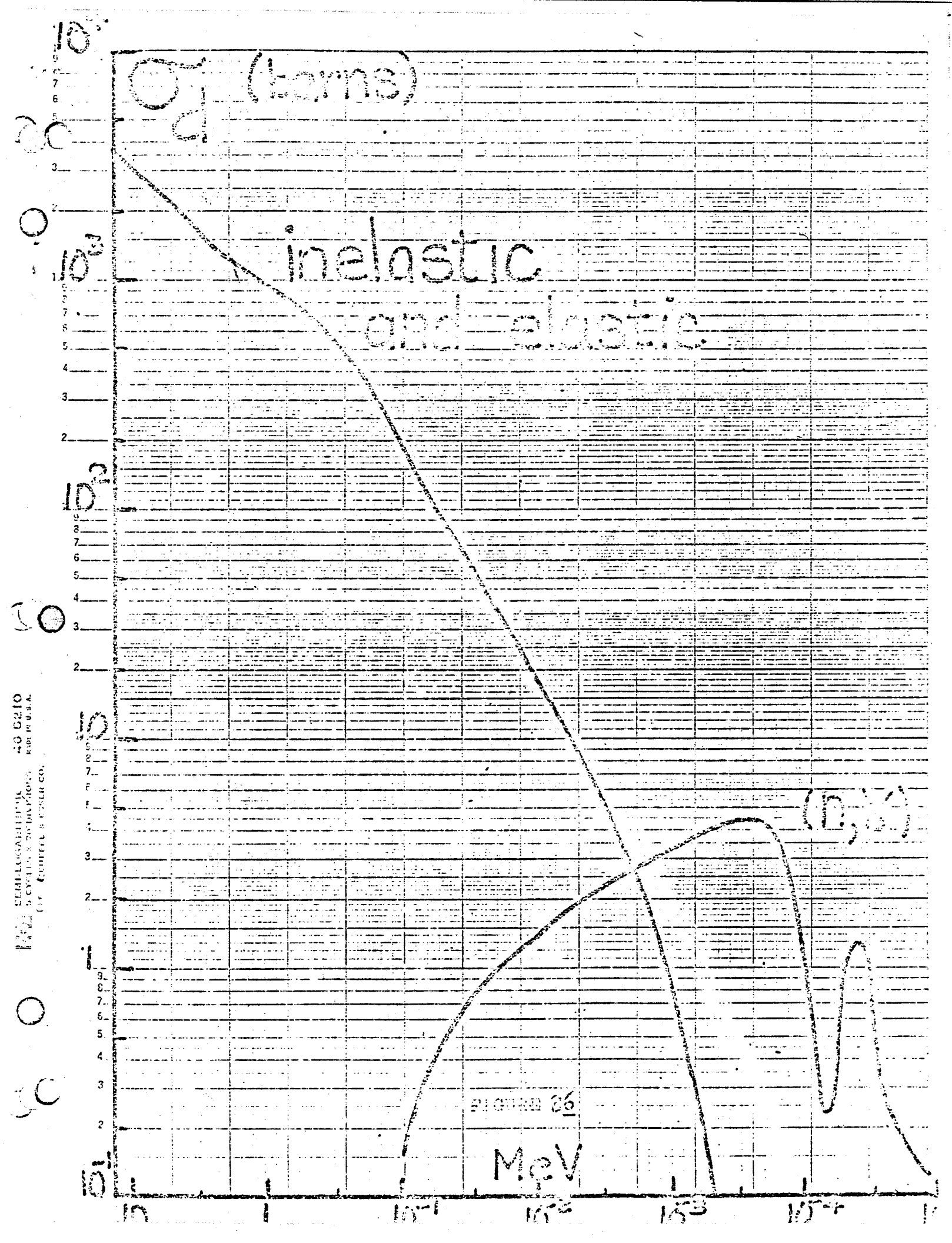
$\sigma_{\gamma n}$ (barns)
inelastic
and elastic
(p,n)
MeV

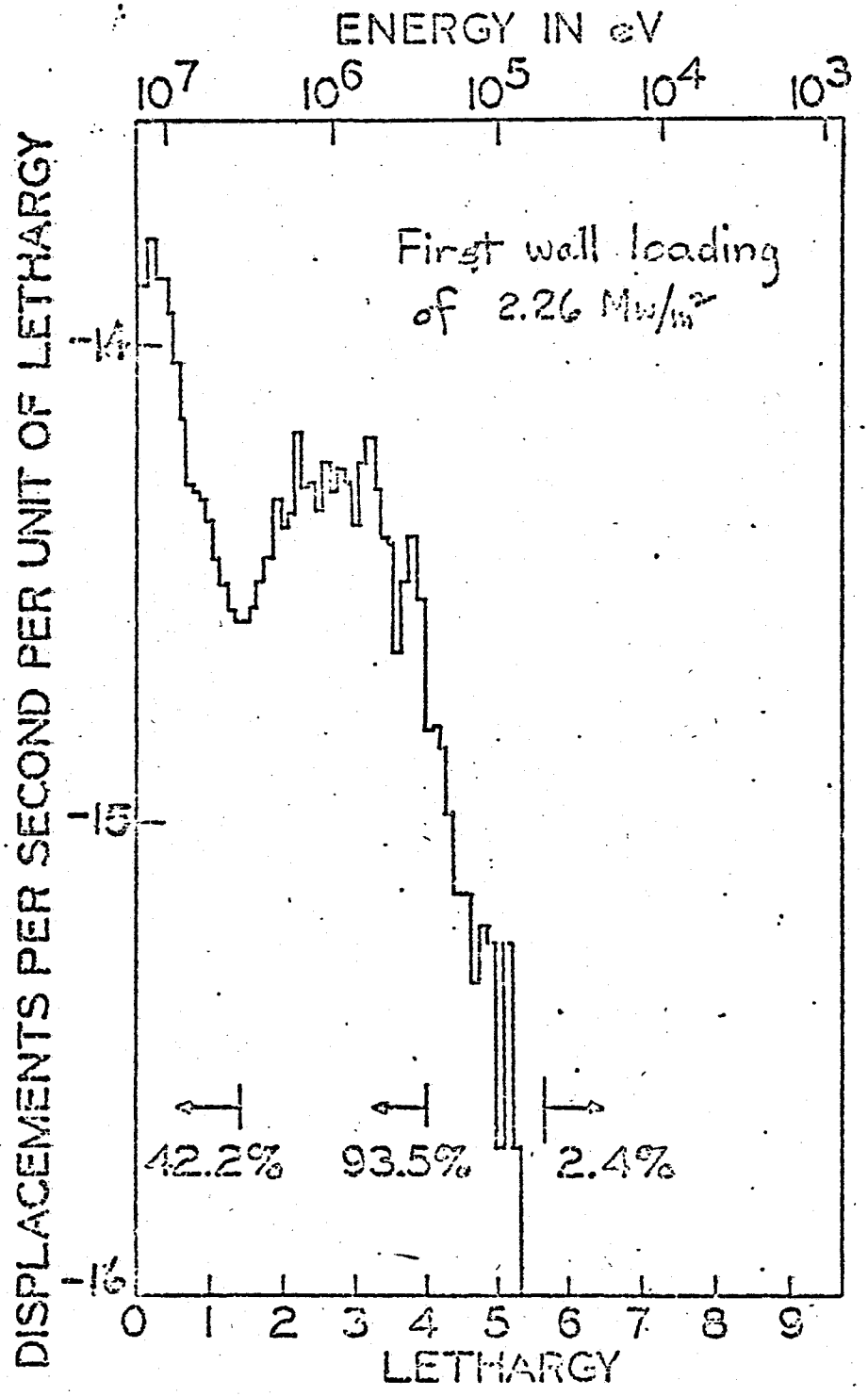
ENERGY IN eV
10^7
10^6
10^5
10^4
10^3
First wall loading of 2.26 Mw/m²
DISPLACEMENTS PER SECOND PER UNIT OF LETHARGY
1/4
1/8
1/16
42.2%
93.5%
2.4%
0 1 2 3 4 5 6 7 8 9
LETHARGY

FIGURE 37

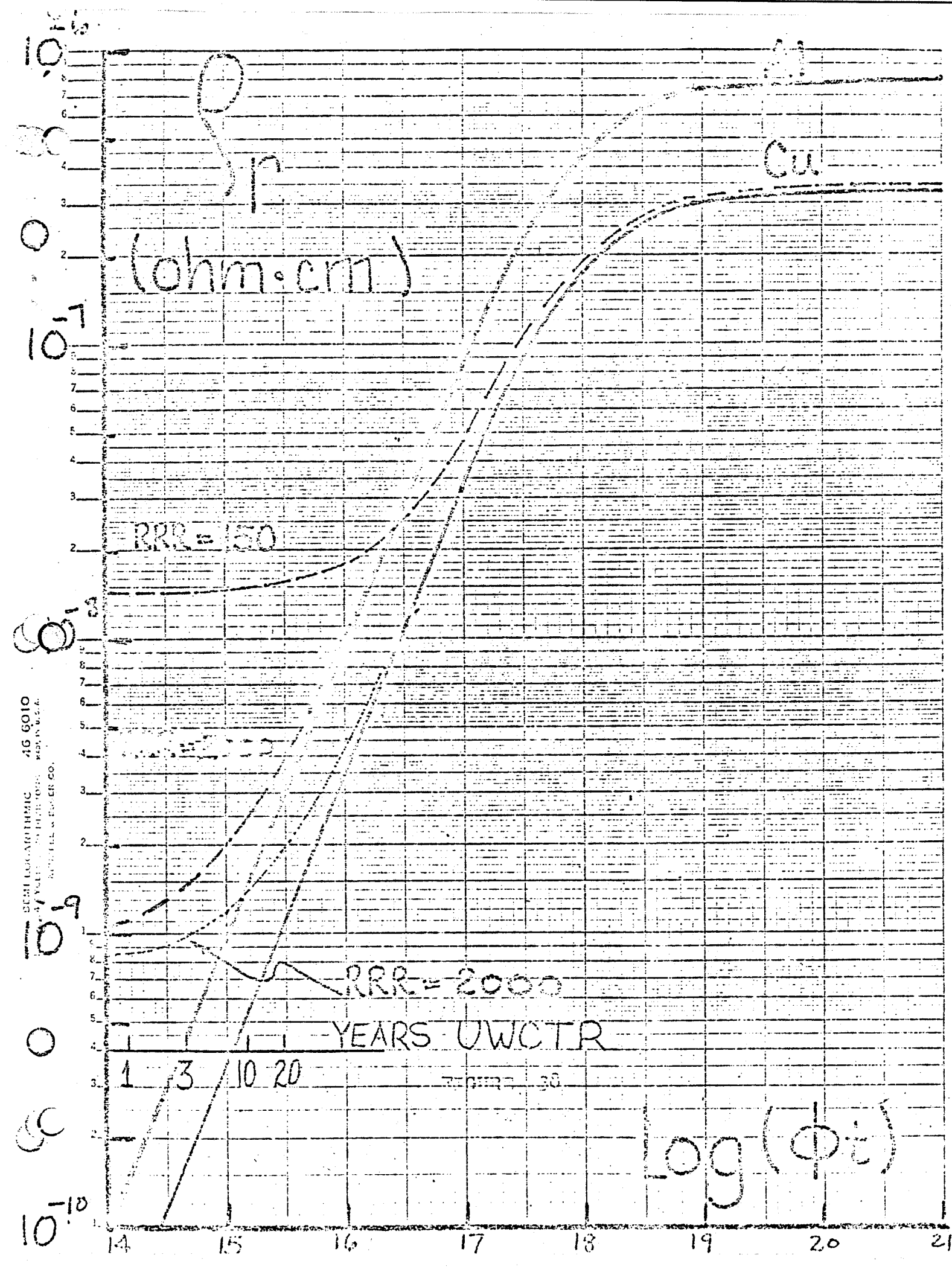
ρ_i (ohm·cm)
Cu
RRR = 150
RRR = 2000
YEARS UWCTR
1 3 10 20
10^{-9}
10^{-10}
14 15 16 17 18 19 20 21
log (ϕ_t)